

1 **Genetic-epigenetic interactions in paternal transgenerational inheritance of metabolic**
2 **disorders**

3 Anne-Sophie Pepin¹, Christine Lafleur², Romain Lambrot², Vanessa Dumeaux³, Sarah
4 Kimmins^{1,2,4*}

5
6 ¹Department of Pharmacology and Therapeutics, Faculty of Medicine, McGill University,
7 Montreal, QC H3G 1Y6, Canada

8 ²Department of Animal Science, Faculty of Agricultural and Environmental Sciences, McGill
9 University, Montreal, QC H9X 3V9, Canada

10 ³Department of Biology, PERFORM Center, Concordia University, Montreal, QC H4B 1R6,
11 Canada

12 ⁴Lead Contact

13 *Correspondence: sarah.kimmins@mcgill.ca

14

15 **Running title:** Paternal obesity alters sperm H3K4me3 and metabolic outcomes in descendants

16

17 **Summary sentence:** Paternal obesity impacts sperm H3K4me3 and is associated with placenta,
18 embryonic and metabolic outcomes in descendants.

19

20 **Keywords:** obesity, metabolism, chromatin, sperm, epigenetic inheritance

21 **ABSTRACT**

22 Parental environmental exposures can strongly influence descendant risks for adult disease.
23 Metabolic disorders arise from the intersection of environmental and genetic risk factors, with
24 epigenetic inheritance being at the center of the familial cycle of transgenerational disease. How
25 paternal high-fat diet changes the sperm chromatin leading to the acquisition of metabolic disease
26 in offspring remains controversial and ill-defined. Using a genetic model of epigenetic inheritance,
27 we investigated the role of histone H3 lysine 4 methylation (H3K4me3) in the paternal
28 transmission of metabolic dysfunction. We show that obesity-induced alterations in sperm
29 H3K4me3 associated with offspring phenotypes and corresponded to embryonic and placental
30 chromatin profiles and gene expression. Transgenerational susceptibility to metabolic disease was
31 only observed when grandsires had a pre-existing genetic predisposition to metabolic dysfunction
32 that was associated with enhanced alterations to sperm H3K4me3. This non-DNA based
33 knowledge of inheritance has the potential to improve our understanding of how environment
34 shapes heritability and may lead to novel routes for the prevention of disease.

35 **INTRODUCTION**

36 The prevalence of obesity and type II diabetes is growing globally at rates indicating that
37 environment rather than genes is the principal driver. Exposures to high-fat diet, toxicants or
38 micronutrient deficiency can impact our health and that of future generations (Gernand *et al.*, 2016;
39 Braun, Messerlian and Hauser, 2017; Donkin and Barrès, 2018; Eberle *et al.*, 2020). Only now are
40 we beginning to identify mechanisms linking these exposures to parental and offspring health. One
41 connection between environment and health is the epigenome. The epigenome refers to the
42 biochemical content associated with DNA that impacts gene expression, chromatin organization,
43 and is transmitted via the gametes to alter phenotypes across generations. Uncovering how

44 genomic information is organized and regulated through epigenetic processes to control gene
45 expression and cell functions in the next generation is still in a nascent stage. We and others have
46 shown that errors in epigenomic profiles in sperm can be induced by environmental exposure to
47 toxicants such as those in insecticides and plastics, obesity, and poor diet (Lambrot *et al.*, 2013;
48 Radford *et al.*, 2014; Donkin *et al.*, 2016; Wu *et al.*, 2017; Lismer, Dumeaux, *et al.*, 2021; Pilsner
49 *et al.*, 2021). We recently demonstrated that these epigenome changes at the level of chromatin
50 can be transmitted via sperm to alter embryonic gene expression, development, and offspring
51 health (Lismer, Dumeaux, *et al.*, 2021). Parental health and fertility historically have focused
52 predominantly on the mother, although it is clear a father's health and lifestyle can also impact his
53 children's health. How epimutations in sperm functionally impact the embryo urgently require
54 elucidation to prevent transmission of disease from Father to offspring.

55
56 Metabolic disease including obesity and type II diabetes can in part be attributed to genetic factors
57 with a 5-10% increased risk (Voight *et al.*, 2010). The remaining risk is attributable to
58 environmental-epigenetic interactions including potentially those of our ancestors. This possibility
59 is supported by epidemiology and animal studies. For example, paternal diets high in fat and
60 associated with glucose intolerance and obesity, or low in folate, or protein, can alter phenotypes
61 in offspring, including metabolism (Carone *et al.*, 2010; Ng *et al.*, 2010; Lambrot *et al.*, 2013).
62 Transgenerational effects are suggested by epidemiological studies in humans that linked the food
63 supply of grandfathers to obesity and cardiovascular disease in their grandchildren (Kaati, Bygren
64 and Edvinsson, 2002; Pembrey *et al.*, 2006; Lumey and Poppel, 2013). Yet the ability for diet to
65 induce similar transgenerational effects in animal models remains controversial with some studies
66 indicating that multigenerational phenotypes are dependent on genetic-epigenetic interactions

67 (Siklenka *et al.*, 2015; Dalgaard *et al.*, 2016; Miska and Ferguson-smith, 2016). Prior studies have
68 shown that exposure of male mice to a high-fat diet altered the sperm epigenome at the level of
69 DNA methylation (Wei *et al.*, 2014), and the metabolic phenotype of the offspring (Ng *et al.*, 2010;
70 Wei *et al.*, 2014). In a similar study, offspring of males fed a low-protein diet (11% versus 20%)
71 had altered cholesterol and lipid synthesis (Carone *et al.*, 2010). Most studies on nutrition, obesity
72 and the sperm epigenome, have focused on the sperm DNA methylome and ncRNA as the potential
73 sperm-borne mediators of metabolic disease (Carone *et al.*, 2010; Radford *et al.*, 2014; Grandjean
74 *et al.*, 2015; Chen *et al.*, 2016; Cropley *et al.*, 2016; de Castro Barbosa *et al.*, 2016; Sharma *et al.*,
75 2016). The role of sperm histone modifications in the transmission of metabolic phenotypes
76 remains unknown.

77

78 Diets high in fat alter epigenetic programming (Ng *et al.*, 2010), likely through the alteration of
79 cellular metabolism, which influences the availability of methyl donors and/or the activation or
80 inactivation of chromatin modifying enzymes . In overweight and obese individuals, homocysteine
81 is consistently elevated, and associated with reduced B12 and folate (Sánchez-Margalet *et al.*,
82 2002; Karatela and Sainani, 2009). In mammals, spermatogenesis is a highly rapid form of cell
83 division that proceeds from the least differentiated spermatogonia to mature spermatozoa. This
84 process is accompanied by dynamic changes to the sperm epigenome including histone
85 methylation which is susceptible to alterations induced by changes in methyl donor availability
86 (Lambrot *et al.*, 2013; Lismer, Dumeaux, *et al.*, 2021). Retained histones are conserved across
87 species from mice to men and are found at the gene regulatory regions implicated in
88 spermatogenesis, sperm function, embryo development, metabolism and routine cellular processes
89 (Hammoud *et al.*, 2009; Lambrot *et al.*, 2019).

90
91 We have shown in human and mouse sperm, histone H3 lysine 4 dimethylation (H3K4me2) and
92 trimethylation (H3K4me3) localize to genes involved in metabolism and development (Lambrot
93 *et al.*, 2019; Lambrot, 2021; Lismer, Dumeaux, *et al.*, 2021). We and others have suggested that
94 histones in sperm may directly influence embryonic gene expression, development, and adult-
95 onset disease. In our prior studies, we aimed to determine whether sperm H3K4me served a
96 function in embryonic development and gene expression (Siklenka *et al.*, 2015; Lismer *et al.*,
97 2020). We generated transgenic mice that overexpressed the histone lysine demethylase KDM1A
98 in developing sperm only. Overexpression of KDM1A during spermatogenesis led to differential
99 enrichment of H3K4me1/2/3 at sperm promoters and enhancers. Offspring sired by KDM1A
100 transgenics had early postnatal death, and severe developmental abnormalities (Siklenka *et al.*,
101 2015). Differentially enriched H3K4me1/2/3 at promoters and enhancers in sperm was associated
102 with altered embryonic gene expression (Siklenka *et al.*, 2015; Lismer *et al.*, 2020).

103
104 The association of histone modifications in sperm with offspring phenotypes has since been
105 confirmed in other mouse models (Stringer *et al.*, 2018; Lesch *et al.*, 2019). The next challenge
106 for the field of epigenetic inheritance was to show that histones in the embryo are paternally
107 inherited and can be altered by exposures. We utilized a folate deficient diet (FD) that changes
108 methyl donor availability and in turn altered histone H3K4me3 in sperm at developmental genes
109 and putative enhancers. A subset of H3K4me3 alterations in sperm were retained in the pre-
110 implantation embryo and associated with deregulated embryonic gene expression. These findings
111 suggest that environmental exposure such as FD alters paternal H3K4me3 which is transmitted to
112 the embryo and influences gene expression and development (Lismer, Dumeaux, *et al.*, 2021).

113

114 In this study, we aimed to assess the non-genetic and genetic impact of high-fat diet (HFD) on the
115 paternal origins of adult-onset metabolic disorders across generations. We used wildtype (WT) or
116 KDM1A-overexpressing transgenic (TG) mice, in combination with a diet-induced obesity model
117 to investigate the following questions: 1) Are inherited metabolic phenotypes associated with
118 altered sperm histone H3K4me3 profiles?; 2) Do metabolic changes induced by an obese paternal
119 diet span generations, or is transgenerational inheritance dependent on genetic-epigenetic
120 interactions?; and 3) Do exposure-induced changes in sperm H3K4me3 enrichment associate with
121 embryonic, placenta and liver function in adult-onset of metabolic disease? We demonstrate that
122 a postnatal paternal high-fat diet induces F₀ obesity and metabolic dysfunction in the F₁.
123 Transgenerational phenotypes were observed only in the obese KDM1A TG F₂ descendants
124 indicating the involvement of genetic-epigenetic interactions in ancestral effects. Obesity-induced
125 alterations in sperm H3K4me3 were predominantly located within 1 kilobase from the TSS and in
126 intergenic regions. Gene ontology (GO) analysis revealed differentially enriched H3K4me3
127 (deH3K4me3) genes were involved in development, placenta formation, inflammatory processes,
128 glucose and lipid metabolic pathways. These enriched pathways are concordant with the metabolic
129 phenotypes observed in offspring. There was no clear relationship between sperm regions bearing
130 altered H3K4me3 and altered liver gene expression. However, embryonic and placenta gene
131 expression patterns overlapped with sperm H3K4me3 alterations suggesting developmental
132 origins of adult-onset metabolic dysfunction.

133

134

135 **METHODS**

136 **Resource availability**

137 *Lead contact*

138 Further information and requests for resources and reagents should be directed to and will be
139 fulfilled by the Lead Contact, Sarah Kimmins (sarah.kimmins@mcgill.ca).

140 *Materials availability*

141 This study did not generate new unique reagents.

142 *Data and code availability*

143 The sperm H3K4me3 ChIP-Seq and liver RNA-Seq data generated during this study are available
144 at the following GEO accession number: GSE178096.

145 **Experimental model and subject details**

146 *Animals*

147 All animal procedures were carried out in accordance with the guidelines of the Faculty Animal
148 Care Committee of McGill University, Montreal. For the wild-type line (WT), C57BL/6NCrl 8-
149 week old males and 6-week old females were purchased from Charles Rivers Laboratory and were
150 allowed one week of acclimation before breeding. For the KDM1A transgenic line (TG), mice
151 were generated as previously described (Siklenka et al., 2015), with the same genetic background
152 as the wild-type line. Single males were housed with two females to generate the F₀ generation.
153 All animals were given access to water and food *ad libitum* and were maintained on a controlled
154 light/dark cycle.

155 **Methods details**

156 *Diet experiments and animal breeding*

157 The low-fat diet (LFD; D12450J) and high-fat diet (HFD; D12492) were obtained from Research
158 Diets, and selected based on the matched amounts of sucrose, vitamin mix and folate. Diets’
159 macronutrients composition are listed in Table S1. Males of the F₀ generation were generated from
160 at least 7 different sires per group. F₀ males were weaned at 3 weeks of age and randomly assigned
161 to either a LFD or HFD (WT LFD: n=17 animals, TG LFD: n=15 animals, WT HFD: n=24
162 animals, TG HFD: n=25 animals). Total body weights were monitored weekly. Cumulative caloric
163 intake was recorded weekly by weighting pellets from the food hopper and calculated as kilocalorie
164 per animal. The diet intervention spanned 10-12 weeks followed by 2 weeks of metabolic testing
165 (at 4 months of age), 1 week of rest and 1-2 weeks of breeding with 7-week old C57BL/6NCrI
166 females. In order to minimize maternal exposure to the intervention diets, females were housed
167 with males overnight and separated during the day, for a maximum of 3 nights per week for 2
168 weeks, or until a vaginal plug was detected. The same timeline was used to generate the F₁ and F₂
169 animals. All females used for breeding and all F₁ and F₂ were fed a regular chow diet (2020X
170 Teklad global soy protein-free extruded rodent diet, Envigo). All animals were sacrificed at 22
171 weeks (\pm 2 weeks) by carbon dioxide asphyxiation under isoflurane anesthesia.

172 ***Metabolic testing***

173 The number of animals per group, per sex and per generation, used for all metabolic
174 characterization tests can be found in Table S2. Assessment of metabolic parameters was
175 conducted at 4 months of age within 2 consecutive weeks according to the standard operating
176 procedures of the NIH mouse Metabolic Phenotyping Center (Ayala *et al.*, 2010). For the glucose
177 tolerance test, animals were fasted overnight for 15 hours (\pm 1 hour) starting at 6:00PM with free
178 access to water. Blood glucose was measured before and 15, 30, 60 and 120 minutes following an
179 intraperitoneal injection of 2 g/kg of a 20% glucose solution (D-glucose, G7021, Sigma Aldrich)

180 with one drop of blood from the tail-tip using a glucometer (Accu-Chek Aviva Nano). For the
181 insulin tolerance test, animals were fasted for 6 hours (1 hour), starting at 9:00AM with free access
182 to water. Blood glucose was measured before and 15, 30, 60 and 120 minutes following an
183 intraperitoneal injection of 1 IU/kg insulin (Insulin solution, I9278, Sigma Aldrich), with one drop
184 of blood from the tail-tip using a glucometer (Accu-Chek Aviva Nano). The area under the curves
185 (AUCs) for the tolerance tests were calculated using the trapezoidal rule (GraphPad Prism version
186 8). For the baseline blood glucose levels, blood glucose levels were measured after an overnight
187 fasting of 15 hours (\pm 1 hour) with one drop of blood from the tail-tip using a glucometer (Accu-
188 Chek Aviva Nano).

189 ***Tissue collection***

190 At necropsy, mice were dissected to collect adipose tissue (gonadal and mesenteric white adipose
191 depots; gWAT and mWAT, respectively) and a liver lobe (left lateral lobe or *lobus hepatis sinister*
192 *lateralis* for RNA-sequencing). All tissues were weighed, transferred to a clean tube, snap frozen
193 in liquid nitrogen and stored at -80°C until subsequent downstream experiments. Cauda
194 epididymides were weighed and immediately used for sperm isolation.

195 ***Sperm isolation***

196 Spermatozoa were isolated from paired caudal epididymides (Hisano *et al.*, 2013; Lismer,
197 Lambrot, *et al.*, 2021). Cauda epididymides were cut into 5 mL of freshly-prepared Donners
198 medium (25 mM NaHCO_3 , 20 mg ml^{-1} BSA, 1 mM sodium pyruvate, 0.53% vol/vol sodium DL-
199 lactate in Donners stock) and gently agitated to allow to swim out for 1 hour at 37°C . The solution
200 was passed through a 40- μm cell strainer (Fisher Scientific, #22363547) and washed three times
201 with phosphate-buffered saline (PBS). The sperm pellet was cryopreserved in freezing medium

202 (Irvine Scientific, cat. #90128) and kept in a -80°C freezer until the chromatin
203 immunoprecipitation experiment.

204 ***RNA-Sequencing and library preparation***

205 RNA extraction was performed using the RNeasy Mini Kit (Qiagen, cat. #74104) following the
206 manufacturer's protocol with slight modifications. In brief, 15-20 mg of liver lobes were cut on
207 dry ice using a sterile scalpel and Petri dish. Samples were lysed in 350 µL of a denaturing buffer
208 (*Buffer RLT* with beta-mercaptoethanol) and homogenized with homogenizer pestles. Lysates
209 were centrifuged at maximum speed for 3 minutes and the supernatants transferred to a clear tube.
210 Ethanol (50%) was added to lysates to promote selective binding of RNA molecules to the silica-
211 based membrane when applied to the spin columns. To avoid genomic DNA contamination, an
212 additional DNase digestion was performed. Finally, membranes of the spin columns were washed
213 twice with 500 µL of *Buffer RPE* and total RNA was eluted using 30 µL of RNase-free water.
214 Libraries were prepared and sequenced at the *Génomique Québec Innovation Centre* with single-end
215 50 base-pair reads on the illumina HiSeq 4000 and paired-end 100 base-pair reads on the illumina
216 NovaSeq 6000 S2 sequencing platforms.

217 ***ChIP-Sequencing and library preparation***

218 Chromatin immunoprecipitation was performed as we have previously described (Hisano *et al.*,
219 2013; Lismer, Lambrot, *et al.*, 2021). In brief, spermatozoa samples in freezing media were thawed
220 on ice and washed with 1 mL phosphate-buffered saline. For each sample, two aliquots of 10 µL
221 were used to count spermatozoa in a hemocytometer under microscope, and 10 million
222 spermatozoa were used per experiment. Sperm chromatin was decondensed in 1 M dithiothreitol
223 (DTT; Bio Shop, #3483-12-3) and the reaction quenched with N-ethylmaleimide (NEM). Samples
224 were lysed in lysis buffer (0.3M sucrose, 60mM KCl, 15mM Tris-HCl pH 7.5, 0.5mM DTT, 5mM

225 MgCl₂, 0.1mM EGTA, 1% deoxycholate and 0.5% NP40). An MNase enzyme (15 units; Roche,
226 #10107921001) was added to aliquots containing 2 million spermatozoa in an MNase buffer (0.3
227 M sucrose, 85 mM Tris-HCl pH 7.5, 3mM MgCl₂ and 2 mM CaCl₂), for exactly 5 minutes at 37°C.
228 The digestion was stopped with 5 mM EDTA. Samples were centrifuged at maximum speed for
229 10 minutes, and the supernatants of aliquots from each sample were pooled back together. Each
230 tube was supplemented with a protease inhibitor to obtain an 1X solution (complete Tablets
231 EASYpack, Roche, #04693116001). Magnetic beads (DynaBeads, Protein A, Thermo Fisher
232 Scientific, #10002D) were pre-blocked in a 0.5% Bovine Serum Albumin (BSA, Sigma Aldrich,
233 #BP1600-100) solution for 4 hours at 4°C and then used to pre-clear the chromatin for 1 hour at
234 4°C. Pulling down of the pre-cleared chromatin was performed with the use of magnetic beads
235 that were previously incubated with 5 µg of antibody (Histone H3 Lysine 4 trimethylation;
236 H3K4me₃; Cell Signaling Technology, cat. #9751) for 8 hours at 4°C. Immunoprecipitation of the
237 chromatin with the beads-antibody suspension was performed overnight at 4°C. Beads bound to
238 the chromatin were subjected to a 3-step wash, one wash with Washing Buffer A (50 mM Tris-
239 HCl pH 7.5, 10 mM EDTA, 75 mM NaCl) and two washes with Washing Buffer B (50 mM Tris-
240 HCl pH 7.5, 10 mM EDTA, 125 mM NaCl). The chromatin was eluted in 250 µL of Elution Buffer
241 (0.1 M NaHCO₃, 0.2% SDS, 5 mM DTT) by incubating the beads twice (2 x 125 µL) shaking at
242 400 rpm for 10 minutes at 65°C, vortexing vigorously and transferring the chromatin elute in a
243 clean tube. The eluted chromatin was finally treated with 5 µL of RNase A (Sigma Aldrich,
244 #10109169001) by shaking in a thermomixer at 400 rpm for 1 hour at 37°C, and then with 5 µL
245 of Proteinase K (Sigma Aldrich, #P2308) overnight at 55°C. DNA was extracted and purified using
246 the *ChIP DNA Clean and Concentrator kit* (Zymo Research, #D5201) using the manufacturer's
247 protocol, eluted with 25 µL of the provided elution buffer. Size selection of the mononucleosomes

248 (147 bp) was performed with the use of Agencourt AMPure XP beads (Beckman Coulter,
249 #A63880). Libraries were prepared in-house using the Ultra-low Input Library kit (Qiagen;
250 #180495). Libraries were sequenced with single-end 50 base-pair reads on the illumina HiSeq
251 4000 sequencing platform (n=5 samples per experimental group).

252 ***Pre-processing***

253 *Liver RNA-Sequencing data*

254 All samples were processed with the same parameters with the exception of those sequenced on
255 the NovaSeq platform to adapt for paired-end sequencing and sequencing read length. Reads were
256 trimmed using *Trim Galore* (version 0.5.0, parameters for HiSeq: --phred33 --length 36 -q 5 --
257 stringency 1 -e 0.1; parameters for NovaSeq: --paired --retain_unpaired --phred33 --length 36 -q 5
258 --stringency 1 -e 0.1) (Krueger, 2015). Trimmed reads were aligned to the *Ensembl* Genome
259 Reference Consortium mouse reference 38 (GRCm38) primary assembly using *hisat2* (version
260 2.1.0, parameters: -p 8 --dta) (Kim, Langmead and Salzberg, 2015). Aligned files with SAM
261 format were converted to binary SAM format (BAM) and sorted by genomic position using
262 *SAMtools* (version 1.9) (Li *et al.*, 2009). Transcripts were assembled and gene abundances
263 calculated using *Stringtie* (version 2.1.2, parameters: -p 8 -e -B -A) (Pertea *et al.*, 2015).

264 *Sperm ChIP-Sequencing data*

265 Sequencing reads were trimmed using *Trimmomatic* on single-end mode to remove adapters and
266 filter out low-quality reads (version 0.36, parameters: 2:30:15 LEADING:30 TRAILING:30)
267 (Bolger, Lohse and Usadel, 2014). Trimmed reads were aligned to the *Mus Musculus* mm10
268 genome assembly using *Bowtie2* (version 2.3.4) (Salzberg, 2013). Unmapped reads were removed
269 using *SAMtools* (version 1.9) (Li *et al.*, 2009), and those with 3 mismatches or more were filtered
270 out using *Perlcoding*. BAM coverage files (BigWig) were generated using *deeptools2 bamCoverage*

271 function (version 3.2.1, parameters: -of bigwig -bs 25 -p 20 --normalizeUsing RPKM -e 160 --
272 ignoreForNormalization chrX) (Ramírez *et al.*, 2016).

273 *Other publicly available ATAC-Sequencing or ChIP-Sequencing datasets*

274 Raw files for 2-cell H3K4me3 and H3K27me3 ChIP-Seq (Liu *et al.*, 2016) (GEO: GSE73952),
275 MII oocyte H3K4me3 ChIP-Seq (Zhang *et al.*, 2016) (GEO: GSE71434), sperm ATAC-Seq (Jung
276 *et al.*, 2017) (GEO: GSE79230), 4-cell and morula ATAC-Seq (Liu *et al.*, 2019) (NCBI SRA:
277 SRP163205), TE H3K4me3 ChIP-Seq (Liu *et al.*, 2016) (GEO: GSE73952), and placenta
278 H3K4me3 ChIP-Seq (Shen *et al.*, 2012) (GEO: GSE29184) were downloaded from the National
279 Centre for Biotechnology Information (NCBI) using the Sequencing Read Archive (SRA) Toolkit.
280 Files were pre-processed as described above for the sperm H3K4me3 ChIP-Sequencing with slight
281 modifications to adapt for datasets with paired-end reads and for different sequencing read lengths.

282 *Other publicly available RNA-Sequencing data*

283 Raw files for 4-cell and morula (Liu *et al.*, 2019) (NCBI SRA: SRP163205), TE (Liu *et al.*, 2016)
284 (GEO: GSE73952), and placenta (Chu *et al.*, 2019) (NCBI SRA: SRP137723) RNA-Seq were
285 downloaded from the National Centre for Biotechnology Information (NCBI) using the
286 Sequencing Read Archive (SRA) Toolkit. Files were pre-processed as described above for the
287 sperm H3K4me3 ChIP-Sequencing with slight modifications to adapt for datasets with paired-end
288 reads and for different sequencing read lengths.

289 *Paternal allele 2-cell embryo ChIP-Sequencing data*

290 Raw files for 2-cell H3K4me3 ChIP-Seq (Zhang *et al.*, 2016) (GEO: GSE71434) were downloaded
291 from the National Centre for Biotechnology Information (NCBI) using the Sequencing Read
292 Archive (SRA) Toolkit. *SNPsplit* (version 0.3.2) was used to build a reference genome with
293 PWK_PhJ SNPs masked (Krueger and Andrews, 2016). Reads were aligned to the generated

294 PWK_PhJ SNPs N-masked reference genome using *Bowtie2* (parameters: -p 10 -t -q -N 1 -L 25 -
295 X 2000 --no-mixed --no-discordant). Aligned files with SAM format were converted to binary
296 SAM format (BAM) and sorted by genomic position using *SAMtools* (version 1.9) (Li *et al.*, 2009).
297 *SNPsplit* (version 0.3.2) was used to assign reads to either the paternal (PWK_PhJ) or the maternal
298 (C57BL/6) genome based on SNPs origin. BAM coverage files (BigWig) were generated using
299 *deeptools2 bamCoverage* function (parameters: -of bigwig -bs 25 -p 20 --normalizeUsing RPKM
300 -e 160 --ignoreForNormalization chrX).

301

302 **Quantification and statistical analysis**

303 *Visualization and statistical analyses for metabolic characterization*

304 Visualization of the metabolic characterization data was performed using Jupyter Notebook
305 (version 6.0.1) with Python (version 3.7.4), with the use of the following packages: *seaborn*
306 (version 0.9.0) (Waskom, 2021), *numpy* (version 1.17.2) (Harris *et al.*, 2020), and *panda* (version
307 0.25.2) (Mckinney, 2010). The *pyplot* and *patches* modules were loaded from the *matplotlib* library
308 (version 3.4.2) (Hunter, 2007). Statistical analyses were conducted using GraphPad Prism 8. For
309 all tests, a p-value less than 0.05 was considered significant. Significance for individual time points
310 on the blood glucose curves for the glucose and insulin tolerance tests, for cumulative energy
311 intake and for growth trajectories during the diet intervention, was tested using multiple t-test with
312 a Holm-Sidak correction. Significance for total body weight, mesenteric and gonadal white
313 adipose tissue weight, baseline blood glucose and the area under the curve for the glucose and
314 insulin tolerance tests, was tested using two-way ANOVA followed by Fisher's LSD.

315 **Bioinformatics analysis**

316 All bioinformatics analyses were conducted using R version 4.0.2 (R Core Team, 2018).

317 ***Liver RNA-Sequencing data***

318 Transcripts with a mean count below 10 were filtered out, conferring a total of 27,907 and 45,992
319 detected expressed transcripts in samples sequenced on the illumina HiSeq and NovaSeq
320 platforms, respectively. Differential expression analysis was conducted using *DESeq2* (version
321 1.28.1) (Love, Huber and Anders, 2014), by including sample's RIN value and group in the design
322 formula. Independent hypothesis weighting (IHW, version 1.16.0) was used to correct for multiple
323 testing and prioritization of hypothesis testing based on covariate (i.e. the means of normalized
324 counts) (Ignatiadis *et al.*, 2016). IHW calculates weight for each individual p-value and then
325 applies the Benjamini-Hochberg (BH) procedure to adjust weighted p-values (Benjamini and
326 Hochberg, 1995). Finally, we used the Lancaster method to perform a gene-level analysis at single
327 transcript resolution (*aggregation* package, version 1.0.1) (Yi *et al.*, 2018). Lancaster applies
328 aggregation of individual transcripts p-values to obtain differentially expressed genes while
329 capturing changes at the transcript level. Genes with a Lancaster p-value below 0.05 were
330 considered significant.

331 For data visualization, transcript counts were normalized using variance stabilizing transformation
332 without the use of blind dispersion estimation (i.e. with parameter *blind=FALSE*) (Love, Huber
333 and Anders, 2014). This transformation approach translates data on a log₂ scale, allows correction
334 for library size and removes the dependence of the variance on the mean (heteroscedasticity).
335 Variance-stabilized transcript counts were corrected for RIN values using *limma's*
336 *removeBatchEffect* function (version 3.44.3) (Ritchie *et al.*, 2015). Pearson correlation heatmaps
337 were generated using the *corrplot* package (version 0.88) (Taiyun, Wei, Simko, 2021), with
338 samples ordered by hierarchical clustering. Principal component analysis was performed using
339 *DEseq's plotPCA* function, with RIN values and sexes labeled. Heatmaps of differentially

340 expressed genes were generated with the *Pheatmap* package (version 1.0.12) (Kolde, 2019), with
341 transcripts ordered by k-means clustering (n kmeans=2) and samples ordered by hierarchical
342 clustering using complete-linkage clustering based on Euclidean distance. Alluvial plots were
343 generated with *ggplot2* (version 3.3.3) (Wickham, 2016), and overlap of differentially expressed
344 genes across genotypes, generations and sexes were determined by the *GeneOverlap* package
345 (version 1.24.0) (Shen, 2014), which uses a Fisher's exact test to compute p-values.

346 *Visualization, Semantic similarity, and Enrichment Analysis of Gene Ontology (ViSEAGO)*

347 Gene ontology (GO) analysis was performed using the *ViSEAGO* package (version 1.2.0)
348 (Brionne, Juanchich and Hennequet-Antier, 2019). Gene symbols and *EntrezGene* IDs from the
349 *org.Mm.eg.db* database were retrieved using the *AnnotationDbi* package. GO annotations were
350 retrieved from *EntrezGene* for the *Mus Musculus* species (ID="10090") using the *ViSEAGO*
351 *EntrezGene2GO* followed by *annotate* functions. ViSEAGO uses topGO to perform GO terms
352 enrichment tests on the sets of genes of interest (differentially expressed genes). We used the
353 Biological Process (BP) ontology category with Fisher's exact test (classic algorithm), and a p-
354 value below 0.01 was considered significant. Results of enrichment tests for each set of genes of
355 interest were then merged and hierarchical clustering was performed based on Wang's semantic
356 similarity distance and *ward.D2* aggregation criterion. Results are visualized on a heatmap where
357 GO terms are ordered by hierarchical clustering based on their functional similarity and GO terms
358 enrichment significance is shown as a color gradient ($-\log_{10}$ p-value) in each set of differentially
359 expressed genes of interest.

360 *Sperm ChIP-Sequencing data*

361 To detect genomic regions enriched with H3K4me3 in sperm, we used *csaw* (version 1.22.1) (Lun
362 and Smyth, 2016) to scan the genome into windows of 150-bp. Windows with a fold-change

363 enrichment of 4 over bins of 2,000 bp (background) were considered enriched. Enriched regions
364 less than 100 bp apart were merged for a maximum width of 5,000 bp, conferring a total of 30,745
365 merged enriched regions. Counts in enriched regions were normalized using TMM normalization
366 followed by *ComBat*'s correction for batch effects (*sva* package, version 3.36.0) (Leek *et al.*, 2012;
367 Zhang, Parmigiani and Johnson, 2020). Spearman correlation heatmaps and MA-plots were
368 generated using raw and normalized counts at enriched regions using *corrplot* (version 0.88)
369 (Taiyun, Wei, Simko, 2021), and *graphics* packages, respectively.

370 Principal component analysis was conducted on normalized counts in enriched regions, by
371 comparing WT HFD vs WT LFD (effect of diet in WT), TG HFD vs TG LFD (effect of diet in
372 TG), and WT LFD vs TG HFD (effects of genotype and HFD). Based on visual assessment of the
373 separation of samples according to dietary or genotype groups along Principal Component 1 (PC1;
374 x axis) or 2 (PC2; y axis), the top 5% regions contributing the PC of interest were selected.

375 Permutational multivariate analysis of variance (PERMANOVA) was conducted to determine
376 whether variation is attributed to dietary/genotype group, using the *adonis* function (*vegan*
377 package, version 2.5-7) (Oksanen *et al.*, 2007). Euclidean distances were used as a metric, 999
378 permutations were performed, and a $p < 0.05$ was considered significant. The directionality change
379 in enrichment was identified based on the positive (up-regulated regions) and negative (down-
380 regulated regions) \log_2 fold change values of the median of normalized counts using *gtools*'
381 *foldchange2logratio* function. Regions with increased and decreased enrichment for each
382 comparison of interest were visualized using *Pheatmap* (version 1.0.12) (Kolde, 2019). Regions
383 distance relative to transcription start site (TSS) were annotated and visualized using the package
384 *chipenrich* (version 2.12.0) (Welch *et al.*, 2014). Gene ontology analysis was performed using
385 *topGO* (version 2.40.0) for genes with increased or decreased H3K4me3 enrichment at the

386 promoter region for each comparison of interest. We used the Biological Process (BP) ontology
387 category with Fisher's exact test *weight01Fisher* algorithm (Alexa, Rahnenführer and Lengauer,
388 2006), and a p-value less than 0.05 was considered significant. Genomic regions with deH3K4me3
389 were annotated using *annotatr* (version 1.14.0) (Cavalcante and Sartor, 2017) including CpG
390 annotations and basic genes genomic features. Upset plots were generated using *UpsetR* (version
391 1.4.0) (Conway, Lex and Gehlenborg, 2017), by ordering each set by frequency and displaying 12
392 sets. Z-scores were calculated using *regioneR's overlapPermTest* (version 1.20.1) which performs
393 a permutation test (n=1,000 permutations) to assess whether a set of regions is significantly
394 enriched to a specific genomic feature compared to genomic regions from the whole genome (Gel
395 *et al.*, 2016). Genome browser snapshots were generated using *trackplot* (Pohl and Beato, 2014).
396 To assess linear trends associated with the cumulative exposure of KDM1A overexpression and
397 high-fat feeding in sperm, we ran *DESeq2* (version 1.28.1) on the top 5% regions contributing to
398 Principal Component 2 (PC2; n=1,538 regions) associated with sample separation when
399 comparing WT LFD and TG HFD normalized counts. In the design formula, we included sample's
400 batch information, and assigned a numerical value for each sample based on their group category
401 (WT LFD=1, WT HFD=2, TG LFD=2, TG HFD=3). Independent hypothesis weighting (IHW)
402 was used to correct for multiple testing and prioritization of hypothesis testing based on covariate
403 (i.e. the means of normalized counts) (Ignatiadis *et al.*, 2016). Median of normalized counts were
404 used to depict the increased and decreased trend of significant regions (adjusted p-value less than
405 0.2) across groups recoded on a numerical scale as defined above.

406

407

408 **RESULTS**

409 **Paternal obesity induces transgenerational metabolic phenotypes in a sex-specific manner**
410 **that are enhanced in KDM1A transgenic descendants**

411 *Impact of paternal obesity on offspring bodyweight and fat accrument*

412 Beginning at weaning until 20 weeks, inbred C57BL/6NCr1 control mice (WT), or KDM1A
413 heterozygous transgenics (TG) were fed either a calorie-dense high-fat diet (HFD; 60% kcal fat),
414 or a sucrose- and vitamin-matched low-fat diet (LFD; 10% kcal fat) (Fig. 1A-C and Table S1).
415 Table S2 provides the animal numbers by sex, generation, and genotype for each metabolic
416 analysis. In the 2 weeks post-weaning, F₀ males on the HFD consumed more calories and gained
417 significantly more weight than LFD males irrespective of genotype (Fig. S1A-B). These effects
418 persisted throughout the diet intervention (Fig. S1A-C), with TG HFD males weighing the most at
419 4 months (Fig. S1C_i). This trend continued in the TG male F₁ and F₂ descendants (fed regular
420 chow), with weights being significantly more than the F₁ and F₂ of TG LFD and WT HFD (Fig.
421 S1C_{ii-iii}). Indicating sex-specific responses to paternal obesity, in female descendants the changes
422 in body weight and fat deposition differed from the males (Fig. S1C-E). For example, female F₁
423 HFD descendants showed no changes in body weight, while F₂ TG HFD females weighed more in
424 comparison to F₂ WT HFD females (Fig. S1C_{iv-v}, respectively). Unexpectedly, F₂ WT HFD
425 females weighed less than F₂ WT LFD. To assess fat accrument, we measured visceral mesenteric
426 (mWAT) and gonadal white adipose tissue (gWAT). All male (F₀) on the HFD accumulated more
427 mWAT compared to LFD males, with no genotype effect (Fig. S1D_i). Male and female F₁
428 offspring sired by WT HFD or TG HFD had increased mWAT fat mass compared to WT LFD and
429 TG LFD (Fig. S1D_{ii} and S1D_{iv}, respectively). Strikingly, mWAT stores were greater in TG HFD
430 F₁ and F₂ males and females compared to WT HFD descendants (Fig. S1D_{ii-v}). Gonadal fat depots

431 in F₀ males were not impacted by the HFD (gWAT; Fig. S1E_i), while male WT HFD F₁ showed
432 increased gWAT, and TG HFD F₁ did not (gWAT; Fig. S1E_{ii}). In the male F₂, TG HFD descendants
433 had increased gWAT, but not WT HFD (Fig. S1E_{iii}). Consistent with the unusual decrease in body
434 weight in female F₂ WT HFD vs F₂ WT LFD, mWAT and gWAT were also reduced in female F₂
435 WT HFD (Fig. S1D_v and S1E_v, respectively). Perhaps indicative of a sex-specific over-correction
436 in female F₂ to grand-sire obesity. Like for body weight and mWAT, female F₂ TG HFD had
437 increased gWAT in comparison to WT HFD (Fig. S1E_v). Overall analysis of body weight and fat
438 accrument revealed sex-specific responses in descendants with transgenerational effects of
439 paternal obesity being enhanced in the TG HFD descendants of both males and females. In female
440 descendants of obese sires, intergenerational effects were more subtle in the F₁.

441

442 *Impact of paternal obesity on glucose homeostasis*

443 Next, we assessed glucose metabolism and insulin sensitivity by glucose tolerance (GTT), and
444 insulin tolerance tests (ITT). These were conducted following the standard operating procedures
445 of the NIH mouse Metabolic Phenotyping Center (Ayala *et al.*, 2010). First, we assessed the effects
446 of the HFD on baseline fasting blood glucose. Consumption of a HFD resulted in elevated baseline
447 glucose in male (F₀) WT HFD and TG HFD in comparison to WT LFD and TG LFD, respectively
448 (Fig. S2A_i). Male TG HFD descendants (F₁ and F₂), but not WT HFD descendants had
449 significantly elevated fasting blood glucose (Fig. S2A_{ii-iii}). In contrast, the glycemic status of all
450 descendant females (F₁ and F₂) did not differ (Fig. S2A_{iv-v}). The same animals used to assess
451 baseline glucose were then given an intraperitoneal glucose challenge and the rate of glucose
452 disposal measured. Analysis of GTT data showed that F₀ WT HFD and TG HFD were glucose
453 intolerant following glucose injection in comparison to F₀ LFD males as shown by their elevated

454 blood glucose curves that persisted across the time course of 15-120 min (Fig. 1D_i). Note that at
455 T₀, before the glucose challenge, F₀ WT HFD males had significantly elevated blood glucose in
456 comparison to F₀ WT LFD which is in line with the baseline glucose measures (Fig. 1D_i and Fig.
457 S2A_i). In contrast, the T₀ blood glucose levels did not differ between male F₀ TG LFD and F₀ TG
458 HFD even though baseline measures after fasting were significantly different (Fig. 1D_i and Fig.
459 S2A_i). These non-congruent findings are attributable to multiple testing correction to adjust for the
460 high number of simultaneous tests conducted in the analysis of GTT curves. Intergenerational
461 effects of the paternal HFD were apparent as male (F₁) sired by WT HFD and TG HFD were also
462 glucose intolerant (Fig. 1D_{ii}). Indicating that there was enhanced metabolic disruption in the male
463 F₁ TG HFD, elevated glucose levels persisted across the GTT time-course for the F₁ TG HFD but
464 not the F₁ WT HFD. Interestingly, glycemic response impairments persisted in the F₂ generation
465 of male descendants of TG HFD only (Fig. 1D_{iii}). Although fat measures were impacted in female
466 F₁ and F₂ HFD, they did not exhibit glucose impairment (Fig. 1D_{iv-v}). Analysis of the area under
467 the curve (AUC) for the GTT was consistent with the male and female glycemic responses shown
468 in the glucose curves (Fig. S2B_{i-v}). In line with the observed glycemic responses, the insulin
469 tolerance test and the corresponding AUC demonstrated that male F₀ WT HFD and TG HFD were
470 insulin insensitive (Fig. 1E_i and S2C_i). Analysis of the AUC indicated that F₁ WT HFD and F₁ TG
471 HFD were insulin insensitive (Fig. S2C_{ii}). Like the glucose tolerance test, there were more
472 pronounced impairments revealed by the ITT for the F₁ TG HFD in comparison to the F₁ WT HFD
473 and only the F₂ TG HFD showed impaired whole body insulin action (Fig. 1E_{iii} and Fig. S2C_{ii-iii}).
474 Like the GTT, there was no indication of insulin impairment in female HFD F₁ nor F₂ (Fig. 1E_{iv-v},
475 S2C_{iv-v}).

476 To summarize, the effects of paternal high-fat diet on glucose homeostasis were sex-
477 specific; male descendants had impaired glucose homeostasis, whereas females did not. Many
478 factors can influence the outcomes of GTT and ITT measures such as the length of fasting, age
479 and strain of mice (Ayala *et al.*, 2010; Bowe *et al.*, 2012). It is worth considering that even though
480 female descendants of HFD (F₁₋₂) showed alterations in fat accretion but not in glucose
481 homeostasis, there remains the possibility that findings may have been different had measurements
482 been taken after a reduced fasting period, or beyond 4 months of age. Taken together, the
483 assessments of weight and metabolic testing indicate that the TG descendants had enhanced
484 responses to paternal obesity in comparison to WT descendants.

485

486 **Paternal obesity was associated with altered liver gene expression in the F₀-F₁ with unique**
487 **genes being differentially expressed in KDM1A descendants (F₁-F₂)**

488 Obesity and metabolic syndrome contribute to steatosis of the liver which is a central organ for
489 glucose and lipid metabolism. To determine whether the altered metabolic status of HFD sires and
490 their descendants (F₁-F₂) was associated with differential gene expression in the liver, we
491 performed RNA-sequencing on the left lateral lobe (*lobus hepatis sinister lateralis*) of adult mice
492 (F₀-F₂). Sequencing quality was high with most RNA profiles having a Pearson correlation
493 coefficient > 0.8 (Fig. S3A). The initial quality assessment of the data revealed that samples tended
494 to cluster by RNA Integrity Number (RIN), which was corrected for in the differential analysis
495 (Fig. S3B). Interestingly, principal component analysis of sequencing data revealed distinct
496 hepatic transcriptomic profiles between males and females that was independent of experimental
497 group and genotype (Fig. S3C). We compared hepatic transcriptome profiles by diet, sex, genotype
498 and generation using a gene-level analysis at single-transcript resolution (Yi *et al.*, 2018). As

499 expected, obesity was associated with differential liver gene expression. Liver from obese F₀ WT
500 males showed differential expression of 2,136 genes in comparison to non-obese F₀ WT males
501 (Fig. 2A, Lancaster $p < 0.05$). Similarly, when comparing obese F₀ TG to non-obese F₀ TG, 1,476
502 genes were differentially expressed (Fig. 2B, Lancaster $p < 0.05$). Of these differentially expressed
503 genes (DEGs), 448 were commonly altered by obesity in both the F₀ WT and F₀ TG ($p < 0.0001$;
504 Fig. 2i). To identify which genes were altered due to genotype, we compared WT obese to TG
505 obese and identified 524 DEGs, suggesting that obesity had a unique effect in TG mice due to an
506 interaction between diet and genotype (Fig. 2C, Lancaster $p < 0.05$).

507 To determine if the effects of paternal obesity on liver function were intergenerational, we
508 compared the liver transcriptome of male and female F₁. In comparison to F₁ WT LFD and TG
509 LFD males, livers of F₁ WT HFD and TG HFD, showed differential expression of 1,015 and 794
510 genes (Fig. 2D and 2E, respectively, Lancaster $p < 0.05$). A total of 165 DEGs overlapped between
511 F₁ WT and TG ($p < 0.0001$; Fig. 2ii). Of the DEGs between the WT LFD and HFD in the F₁, 139
512 were the same deregulated genes as identified in the F₀ WT LFD vs HFD males ($p = 0.76$; Fig 2iv).
513 Similarly, there were 103 shared transcripts identified as differentially expressed between the F₁
514 TG LFD vs HFD, that were also altered in the F₀ TG LFD vs HFD ($p = 0.003$; Fig 2v). This suggests
515 that a common set of genes maintain dysfunction as a consequence of direct exposures to obesity
516 and these changes are maintained in the non-obese F₁. When comparing genes altered by genotype
517 in the F₁ (WT HFD vs TG HFD), 961 were significantly altered (Fig 2F, Lancaster $p < 0.05$), with
518 78 overlapping DEGs between the F₀ and the F₁ ($p < 0.0001$; Fig 2vi). The overlap in deregulated
519 genes between the F₀ and F₁ indicates that the metabolic phenotypes generated by the paternal
520 HFD persist intergenerationally despite the F₁ being fed a regular chow diet. There were also
521 novel genes in the F₁ that were deregulated, suggesting secondary intergenerational effects of the

522 paternal HFD. As expected, there was a reduction in the number of deregulated genes in the F₁
523 WT and TG males compared to the F₀ which is consistent with the milder metabolic phenotypes
524 observed in the F₁ in comparison to the directly HFD-exposed F₀. Likely reflecting the enhanced
525 genotype influence of the F₀ TG HFD sires that resulted in more severe weight changes and higher
526 baseline glucose in their descendants compared to the WT HFD descendants, there were more
527 DEG in the male F₀ compared to the male F₁ TG HFD (524 in F₀ versus 961 in F₁; Fig. 2_{vi}).

528 The last comparisons in liver transcriptomes were between the F₁ male and female. Despite
529 the female F₁ having no metabolic phenotype detected by our measures, there was significantly
530 altered gene expression in the livers of F₁ female offspring of WT HFD vs WT LFD sires (830;
531 Fig 2G, Lancaster p<0.05) Of these, 153 were in common with the F₁ male WT HFD sired
532 offspring (p<0.0001; Fig 2_{vii}). Likewise, the F₁ female sired by TG HFD had 1,125 DEGs in
533 comparison to females sired by TG LFD (Fig. 2H, Lancaster p<0.05) with 148 in common with F₁
534 male TG HFD sired offspring (p<0.0001; Fig. 2_{viii}). Of these altered transcripts, 160 were in
535 common between F₁ female descendants of WT HFD and TG HFD (p<0.0001; Fig. 2_{iii}). Like the
536 F₁ male TG HFD offspring, there were unique transcripts altered in F₁ female TG HFD offspring
537 (1,370; Fig. 2I, Lancaster p<0.05), with 181 differentially expressed in both F₁ males and females
538 (p=<0.0001; Fig. 2_{ix}). These may reflect genes impacted by genotype regardless of sex. An
539 interesting finding from the F₂ phenotyping was those transgenerational metabolic effects of the
540 HFD were only detected in the male descendants of TG. Therefore, we only profiled F₂ male livers
541 by RNA-seq. This analysis revealed differential expression of 2,141 genes between the F₂ WT
542 HFD and TG HFD (Fig. 2J, Lancaster p<0.05) with 129 overlapping with the F₁ WT HFD vs TG
543 HFD males (p=0.06; Fig 2_x). The number of differentially expressed genes increased every
544 generation in comparisons between the WT HFD and the TG HFD (F₀=524, F₁=961, F₂ = 2,141).

545 This sustained deregulated gene expression in the livers of TG HFD F₂, matches the enhanced
546 metabolic phenotypes observed in only F₂ TG HFD males but not in the F₁ WT HFD. It also
547 indicates a dilution in phenotype by reprogramming in the WT HFD descendants.

548

549 **Paternal diet-induced obesity disrupts gene expression in functional processes that differ**
550 **between genotypes, sex and generations**

551 To gain insight into the physiological implications of obesity-induced altered hepatic
552 transcriptomes, we used a gene ontology (GO) approach combined with functional similarity
553 clustering to compare processes in the liver impacted by diet across genotype and sex, and those
554 impacted by genotype across generation (Fig. 3A-C, Supplemental files 1-3 and Table S3-5)
555 (Brionne, Juanchich and Hennequet-Antier, 2019). Interactive heatmaps that facilitate in-depth
556 probing of the gene frequency and the $-\log_{10}$ p-value of enriched GO terms within each cluster are
557 found in Supplemental files 1-3. The non-interactive heatmaps are shown in Fig. 3. Overall, there
558 were similar processes altered by obesity in F₀ WT and TG livers, including lipid, amino acid, and
559 small molecule metabolism (Fig. 3A, Supplemental file 1 and Table S3; clusters 1-5), homeostasis
560 and environmental responses (clusters 8-10), and cellular differentiation and signalling (clusters
561 11-13). However, the gene frequency (# of genes annotated to that process) within processes
562 differed by genotype. For example, genes involved in lipid metabolic processes (cluster 2),
563 specifically the carboxylic acid metabolic process was more enriched at 19.03% gene frequency
564 in the F₀ WT HFD ($-\log_{10}$ p-value 6.18), than in the F₀ TG HFD at 14.7% gene frequency ($-\log_{10}$
565 p-value 4.37). In contrast, genes involved in environmental responses (cluster 8) such as to alcohol,
566 were similarly enriched in both the F₀ WT HFD with a gene frequency of 19.19% ($-\log_{10}$ p-value
567 1.3) and of 19.19% in the F₀ TG HFD ($-\log_{10}$ p-value 2.29). Interestingly, deregulated genes

568 involved in insulin, protein and metal ion transport were only enriched in F₀ TG HFD livers
569 (clusters 6-7).

570 When the altered functional pathways were compared between F₁ WT LFD vs WT HFD
571 males and females, there were clear impacts of obesity on the liver functional pathways of
572 offspring, and these differed by sex (Fig. 3B, Supplemental file 2 and Table S4). Reflecting sex
573 differences, a greater number of GO terms related to inflammation (cluster 4), and cell cycle,
574 differentiation and signalling regulation (clusters 10-11) were significantly enriched in males
575 compared to females. Of note, genes involved in the regulation of proinflammatory cytokines were
576 particularly enriched in males but not females (clusters 4 and 6). This concurs with the more severe
577 phenotypes observed in the males. Conversely, genes involved in DNA/RNA biosynthesis,
578 transcription factors and telomere activity (clusters 1-3), and macromolecule and nitrogen
579 metabolism (cluster 5) were more enriched in females. Interestingly, pathways associated with
580 chromatin and cellular organization and protein metabolism (clusters 8-9) were differentially
581 enriched by paternal obesity in both sexes.

582 Next, we compared the intergenerational and transgenerational effect of the interaction
583 between the KDM1A transgene with obesity in terms of differences in process enrichment across
584 generations when comparing F₀₋₂ WT HFD with F₀₋₂ TG HFD (Fig. 3C, Supplemental file 3 and
585 Table S5). Reflecting the increasing generational changes in liver gene expression in the TG HFD
586 descendants, there was an increase in the number of significantly enriched GO terms when
587 comparing WT HFD vs TG HFD across generations (F₀ male=79; F₁ male=118; F₁ female=159;
588 F₂ male=206; Supplemental file 4). This finding is concordant with the metabolic phenotypes
589 detected in the TG HFD male F₂ descendants, but not in the F₂ male WT HFD (Fig. 1, Fig. S1, Fig.
590 S2; Fig. 3C and Supplemental file 3). An interesting finding that supports a unique genotype

591 response in the male F₁ TG HFD in comparison to the male F₁ WT HFD, is the over-representation
592 of genes implicated in chromatin remodelling and transcription (clusters 17-19). This may reflect
593 the activation of genetic response to reprogram the KDM1A-diet-induced sperm epimutations. In
594 addition, there was an enrichment in the differential expression of genes with functions related to
595 inflammation and environmental response (clusters 3-5), and metabolic processes (clusters 11-14).
596 Genes involved in lipid catabolic processes (cluster 13) were increasingly enriched across
597 generations, with 3.54% (F₀), 6.69% (F₁ male), 8.66% (F₁ female) and 20.87% (F₂) gene
598 frequency. Like the males, female F₁ WT HFD vs F₁ TG HFD showed differences in enrichment
599 pathways that reflect the interaction between obesity and the KDM1A transgene in the F₀ and the
600 sex differences observed in the phenotypes (Fig. 3C)

601

602 **Obesity in combination with expression of the KDM1A transgene increases differential**
603 **enrichment of sperm H3K4me3 at genes involved in metabolism and development**

604 Previously we associated paternal folate deficient diets with altered H3K4me3 in sperm
605 and showed that these alterations are transmitted to the embryo and in line with offspring
606 phenotypes (Lismer et al., 2021). We hypothesized that the sperm epigenome at the level of
607 H3K4me3 would be altered by obesity and that this effect would be enhanced in KDM1A TG
608 males with pre-existing alterations in sperm H3K4me3. To test these hypotheses, we performed
609 native chromatin immunoprecipitation followed by deep sequencing (ChIP-seq) targeting histone
610 H3K4me3, using sperm from individual WT or TG males fed either a LFD or HFD (N=5 per
611 experimental group, on average 33.3 million reads per sample with an alignment rate of 97%,
612 Table S6). H3K4me3 localized to 30,745 genomic regions, with a Spearman correlation coefficient
613 of 0.98 between samples (Fig. 4A and S4). Principal component analysis of H3K4me3 profiles

614 revealed a clear separation of samples according to dietary treatment within genotype groups (Fig.
615 4 B-C). WT samples separated along Principal Component 1 (PC1) with 37.41% of variance
616 attributed to diet (Fig. 4B; PERMANOVA, permutation-based $p=0.01$). TG samples separated on
617 PC1 with 32.68% of the variability, with diet as the second source of variance (PC2), at 25.56%
618 (Fig. 4C; PERMANOVA, permutation-based $p = 0.009$).

619 To focus our analysis on the regions most impacted by diet we selected the top 5%
620 differentially enriched H3K4me3 regions (deH3K4me3, $n=1,538$) in each genotype (PC1 in WT,
621 PC2 in TG) (Fig. 4Di-iv). The genome distribution analysis for specific annotations showed that
622 diet-sensitive H3K4me3 regions were predominantly located in CpG islands, promoters, exons,
623 and intergenic regions (Fig. S5). To a lesser extent, deH3K4me3 also occurred at transposable
624 elements (LINE, SINE and LTR), where epigenetic de-repression is associated with the use of
625 alternative promoters and long- and short-range enhancers that are implicated in embryo
626 development and pluripotency (Gerdes *et al.*, 2016) (Fig. S5). Representative genome browser
627 tracks (Fig. S5) showing enrichment gains and losses for H3K4me3 at gene promoters are shown
628 for *Pde1c* (phosphodiesterase 1C; affects the olfactory system), *Bcdin3d* (RNA methyltransferase;
629 highly expressed in embryonic development), *Sh2d4a* (Sh2 domain containing protein 4A;
630 expressed during development and associated with endocrine and liver function), and *Coll5a1*
631 (collagen alpha-1; cell differentiation and development, endocrine, cardiovascular system and
632 more) (*Mouse Genome Informatics*, no date).

633 Next, we compared the regions of H3K4me3 that were altered by obesity, their genomic
634 location, directionality change and functions between diets and genotype (Fig. 4). As a response
635 to obesity, H3K4me3 enrichment gains were more predominant than losses for both F₀ WT HFD
636 and TG HFD (Fig. 4D). In the WT HFD 1,323 regions gained and 215 lost H3K4m3 in comparison

637 to the WT LFD (Fig. 4Di-ii). Similarly, in the F₀ TG HFD sperm, 1,067 regions gained and 471
638 lost H3K4me₃ in comparison to the F₀ TG LFD (Fig 4Diii-iv). Regions with deH3K4me₃ in WT
639 HFD had an 15.6% overlap (240/1,538 regions) with those of TG HFD (Fig. 4E). Of those
640 common 240 regions, 162 had the same directionality change in both WT and TG HFD, with 159
641 regions with a gain and 3 regions with a reduction in H3K4me₃ enrichment (Fig. 4 F and G,
642 respectively). The non-overlapping regions of deH3K4me₃ in WT HFD and TG HFD sperm could
643 be a consequence of genetic-epigenetic interactions where the TG mice respond uniquely to
644 obesity as was observed in the phenotypic characterization. The proximity to the TSS of the
645 deH3K4me₃ regions in sperm altered by obesity in the F₀ WT HFD and TG HFD were similar
646 (Fig. 4H).

647 Next, we performed a gene ontology (GO) enrichment analysis on promoters to gain
648 functional insight into the genes disturbed by obesity and how they may relate to offspring
649 phenotypes. This analysis revealed that changes in H3K4me₃ occurred at promoters of genes that
650 function in reproduction and development which is expected as these processes are known to be
651 enriched for H3K4me₃ in sperm (Fig. 4I and Tables S7-10). Supporting the idea that deH3K4me
652 is specifically impacted by obesity and may be implicated in the transmission of metabolic disease
653 to offspring is the finding that enriched genes were identified in processes related to metabolism
654 and the impact of obesity. These included inflammatory processes, glucose and lipid metabolic
655 pathways, and one-carbon cycle metabolism (Fig. 4I_{i-iv}; Tables S7-10). Notably, some of the
656 significantly enriched pathways are concordant with disturbed metabolic phenotypes of the F₀-F₂
657 including, for example, carbohydrate metabolic processes, glycolysis, growth hormone signaling
658 and insulin signaling (Fig 4I, Tables S7-10).

659 The metabolic phenotypes of WT HFD and TG HFD descendants were similar, although
660 the F₁₋₂ TG HFD showed enhanced abnormalities. We hypothesized that these differences in
661 offspring metabolic disturbances may relate to the degree of H3K4me3 alteration in F₀ sperm, the
662 directionality of the change (gain versus loss), and the functionality of genes bearing alterations.
663 Interestingly, when comparing WT LFD with TG HFD sperm, samples separated along PC2, with
664 26.69% of variance associated with genotype and diet (Fig. 5A; PERMANOVA, permutation-
665 based p=0.006). Of the top 5% impacted regions selected (n=1,538), a greater proportion showed
666 a gain of enrichment for H3K4me3 in TG HFD sperm in comparison to WT LFD (Fig. 5B, n=1,071
667 regions with gains; Fig. 5C. n=467 regions with losses). We analyzed the detected regions
668 impacted by genotype and diet (n=1,538) for differential enrichment to determine whether obesity
669 in combination with KDM1A overexpression led to greater changes in H3K4me3 enrichment. This
670 analysis identified 264 regions with a significant linear trend, where TG HFD sperm showed a
671 greater degree of change in enrichment, and TG LFD and WT HFD showed intermediate changes
672 in comparison to WT LFD (Fig. 5D-E, adjusted p<0.2). There were only 9 significant regions
673 with further increase in H3K4me3 in the TG HFD (Fig. 5 D), whereas 255 regions showed a
674 greater loss of H3K4me3 enrichment in the TG HFD (Fig. 5E). Consistent with the stronger
675 metabolic phenotypes observed in the TG HFD F₁₋₂, the functional analysis of the promoters
676 showing significant linear trends (n=104) for H3K4me3 across experimental groups occurred at
677 genes implicated in metabolic and cardiovascular disease progression (Fig. 5F, Table S11).

678

679 **Paternal obesity impacts sperm H3K4me3 at regions that coincide with open chromatin and**
680 **gene expression in pre-implantation embryos**

681 We recently demonstrated that sperm H3K4me3 is transmitted to the embryo and associated with
682 gene expression (Lismer, Dumeaux, *et al.*, 2021). We hypothesized that obesity-altered sperm
683 H3K4me3 is transmitted and associated with chromatin accessibility in the early embryo, which
684 in turn could influence gene expression and offspring phenotypes. To assess this possibility, we
685 investigated the relationship between deH3K4me3 in sperm in relation to H3K4me3 in the embryo,
686 the oocyte and open chromatin (Zhang *et al.*, 2016; Jung *et al.*, 2017; Liu *et al.*, 2019). We used
687 existing datasets from mouse 2-cell embryos (Zhang *et al.*, 2016), generated by crossing males and
688 females of different strains, permitting the assignment of reads to the paternal-specific allele. In
689 line with a preferential paternal contribution of H3K4me3 to the 2-cell embryo, regions enriched
690 for H3K4me3 in sperm, including those altered by obesity are not enriched in the oocyte (Fig 6A).

691 Next, we examined the relationship between sperm H3K4me3, chromatin accessibility and
692 embryonic gene expression at the 4-cell and morula stages (Fig. 6 and Fig. S6A). We focused on
693 the 4-cell and morula stages as this is when large-scale embryonic transcription directs
694 development (Jukam, Shariati and Skotheim, 2017). There is an association between sperm
695 H3K4me3 and embryonic gene expression (Lismer *et al.*, 2020; Lismer, Dumeaux, *et al.*, 2021)
696 (Fig. S6 A_i). Strikingly, sperm H3K4me3 including obesity-sensitive regions are associated with
697 ATAC-seq signal in pre-implantation embryos (Fig. 6A and 6B). To determine the functional
698 relationship between the H3K4me3 obesity-altered regions and embryonic gene expression, we
699 compared these with 4-cell and morula expressed genes and performed a gene ontology analysis.
700 Of the sperm deH3K4me3 regions overlapping promoters (n=738), 51.8% (n=382) are expressed
701 in the 4-cell embryos, 44.3% (n=327) are expressed in the morula embryos, and 39.7% (292)
702 overlap in both (Fig. S6A_{ii}). To gain insight into what obesity-altered H3K4me3 associated genes
703 in sperm relate to embryonic gene expression, we performed a GO analysis on the regions that are

704 deH3K4me3 in sperm and the corresponding genes expressed in 4-cell and morula embryos (Fig.
705 6C_{i-ii}). Again, supporting a role for sperm H3K4me3 in paternal transmission of metabolic disease,
706 with both the 4-cell and the morula gene processes significantly enriched specific to metabolism
707 (Fig. 6C_{i-ii} and Tables S12-13).

708 Unlike our previous studies on the function of H3K4me3 sperm where we found strong
709 associations between deH3K4me3 and birth defects (Lismer *et al.*, 2020; Lismer, Dumeaux, *et al.*,
710 2021), in this study the defects in descendants appear to be limited to metabolic dysfunction and
711 not development. To further probe the bias of obesity altered H3K4me3 for genes that function in
712 metabolism and not post-implantation development, we examined the relationship between
713 deH3K4me3 and H3K4me3/H3K27me3 bivalency. Genes that are bivalent for
714 H3K4me3/H3K27me3 in sperm and embryos are termed as poised genes and are expressed later
715 in embryo development (Hammoud *et al.*, 2009; Brykczynska *et al.*, 2010). Some promoters with
716 high H3K4me3 enrichment in sperm are associated with bivalency in the 2-cell embryos (Fig.
717 S6B_i). The obesity-altered H3K4me3 regions are predominantly not associated with
718 H3K4me3/H3K27me3 bivalent genes in the embryo (Fig. S6C_{ii}). Taken together these findings
719 suggest a preferential contribution of H3K4me3 on the paternal chromatin in the early embryo that
720 includes obesity-sensitive regions that may be instructive of metabolic-associated gene expression
721 and a direct route for epigenetic inheritance.

722

723 **HFD alters the sperm epigenome at regions instructive for placenta development**

724 The placenta is a key extra-embryonic organ that represents the uterine-fetal interface and
725 plays a central role in energy allocation, nutrient exchange, and developmental progression.
726 Placental abnormalities have been linked to late onset cardiometabolic diseases, highlighting the

727 importance of the *in utero* environment for adulthood metabolic health (Perez-Garcia *et al.*, 2018).
728 Our gene ontology analysis on diet-induced deH3K4me3 regions in sperm revealed significant
729 enrichment of genes involved in placenta development (Fig. 4I and Tables S7-10). Given the sperm
730 epigenome influences placental gene expression (Wang *et al.*, 2013), we were interested in the
731 prospect that diet-induced epimutations in sperm affect placenta gene expression that could
732 influence metabolic phenotypes across generations. To investigate this possibility, we used
733 existing H3K4me3 and transcriptomic datasets from mouse trophoctoderm – the embryonic
734 precursor of placenta lineage – and placenta (Shen *et al.*, 2012; Wu *et al.*, 2016; Chu *et al.*, 2019).
735 We compared the enrichment profiles of H3K4me3 in sperm, trophoctoderm and placenta, at all
736 H3K4me3-enriched regions in sperm (n=30,745) and at those sensitive to diet (n=2,836). Most
737 regions showed presence of H3K4me3 in both the trophoctoderm and the placenta (Fig. 7A). Of
738 the 738 deH3K4me3 regions localizing to promoters in sperm, 56.8% (n=418) were expressed in
739 the trophoctoderm, 76.8% (n=567) were expressed in the placenta, and 54.6% (n=403) were
740 expressed in both (Fig. S6Cii). Gene ontology analysis of the shared H3K4me3 in sperm with TE
741 and placenta revealed that there was an association with placenta function including at
742 deH3K4me3 regions (Fig. 7Bi and iii, Tables S14 and S16). The GO analysis of the H3K4me3
743 regions that were not common with TE and placenta were involved in spermatogenesis,
744 fertilization and sperm function (Fig. 7Bii and iv, Tables S15 and S17).

745 Next, we compared gene enrichment of sperm H3K4me3 with low- and high-expressed
746 genes in the TE and placenta. Suggesting an influential role of sperm H3K4me3, the highly
747 expressed genes and to a lesser extent the lowly expressed genes in placenta were positively
748 correlated with sperm H3K4me3 (Fig. 7Ci-iv). Notably when the same comparisons were made
749 with the deH3K4me3 there was a significant relationship with both lowly- and highly-expressed

750 placenta genes ($p=1.2e-11$ and $p=0.008$, respectively; Fig. 7Cv-viii). In addition, the GO analysis
751 of TE- and placenta-expressed genes that overlap with deH3K4me3 promoters are in line with the
752 metabolic phenotypes in offspring (Fig. 7D i-ii, Tables S18-19). Taken together this analysis raises
753 the possibility that obesity-induced alterations in sperm may influence embryonic and placenta
754 gene expression to alter metabolic function of offspring.

755

756 **Obesity-induced sperm epigenomic and hepatic transcriptomic alterations are unrelated**

757 In a recent study, paternal low-protein diet was associated with reduced H3K9me2 at genes in
758 sperm and were suggested to modulate gene expression profiles in the liver (Yoshida *et al.*, 2020).
759 We aimed to assess whether a similar association between obesity-induced deH3K4me3 in sperm
760 would relate to differential expression in the livers of the next generation. We focused on the
761 obesity-associated sperm deH3K4me3 at promoters in F₀ sires and their relationship to
762 differentially expressed genes in the liver (DEGs) of F₁ males. This analysis revealed that genes
763 with differential expression in livers ($n=1,644$) were by in large unrelated to genes bearing
764 deH3K4me3 in sperm. Only 9.1% ($n=67$) of promoters with deH3K4me3 in sperm were
765 differentially expressed in the liver of F₁ males sired by HFD-fed sires (Fig. S7 A-B). We then
766 asked if deH3K4me3 promoters in sperm and liver DEGs had related biological functions.
767 Strikingly, sperm- and liver-altered genes showed few functional similarities (Fig. S7C,
768 Supplemental file 5 and Table S20). Functional pathways specifically enriched in deH3K4me3
769 promoters involved development and differentiation processes (clusters 12-15). As expected in a
770 paternal obesity model, gene processes altered in offspring livers included: regulation of
771 transcription and RNA splicing (clusters 1-3), protein and histone post-translational modifications
772 (clusters 4-5), and metabolism of lipid, nitrogen and glucose (clusters 6-8). Pathways enriched in

773 both the deH3K4me3 promoters in sperm and the DEGs in liver were involved in cell cycle,
774 transport and signaling (clusters 16-19), and response to stress and inflammation (clusters 20-22).
775 These commonly enriched pathways might reflect obesity-associated systemic inflammation
776 which could affect multiple organs in a similar manner. These findings indicate that paternal
777 obesity alters the sperm epigenome at distinct genes and functional pathways than those
778 differentially expressed in offspring livers and fits with a developmental origin of adult metabolic
779 dysfunction that could be related to alterations in gene expression in the embryo and placenta.

780

781 **DISCUSSION**

782 Epidemiological studies and animal models point to the world-wide increases in childhood obesity
783 and diabetes being in part attributed to environment-epigenetic interactions in the gametes
784 (Huypens *et al.*, 2016; Isganaitis, Suehiro and Cardona, 2017; Sales, Ferguson-Smith and Patti,
785 2017). With the prevalence of childhood obesity predicted to reach 70 million by 2025 (Brown *et*
786 *al.*, 2015), it is urgent to gain a better understanding of the underlying heritable mechanisms.
787 Studies of obesity in mice and men have focussed on the role of sperm DNA methylation and non-
788 coding RNA as mediators of paternal non-genetic inheritance of metabolic dysfunction (Carone *et*
789 *al.*, 2010; Fullston *et al.*, 2013; Lambrot *et al.*, 2013; Martínez *et al.*, 2014; Chen *et al.*, 2016;
790 Soubry *et al.*, 2016; Youngson *et al.*, 2016; Zhang *et al.*, 2018; Salas-Huetos *et al.*, 2021). At the
791 mechanistic level, how sperm altered DNA methylation and non-coding RNA lead to metabolic
792 phenotypes in offspring remains unresolved. In contrast to the voluminous studies on the response
793 of sperm DNA methylation to paternal obesity/diets, there have been only a handful of studies on
794 the role of chromatin. The few chromatin studies have been limited by either the state of the

795 available technology, methodology used, or gene targeting approaches (Carone *et al.*, 2011;
796 Palmer *et al.*, 2011; Martínez *et al.*, 2014; Donkin *et al.*, 2016).

797 Here we focused on sperm chromatin, specifically histone H3K4me3, as we have shown
798 previously that it is impacted by the environment, is transmitted to the embryo, and functions in
799 transgenerational inheritance (Lismer *et al.*, 2020; Lismer, Dumeaux, *et al.*, 2021). Our findings
800 implicate obesity-induced alterations in H3K4me3, in the transmission of metabolic disease. The
801 effects of obesity on the paternal epigenome were specific and linked with the metabolic
802 dysfunction in the descendants; deH3K4me3 occurred at the promoters of genes involved in
803 fertility, metabolism, and placenta processes. Indicative of paternal transmission of sperm altered
804 H3K4me3 as a mechanism of metabolic dysfunction was the strong relationship between
805 deH3K4me3, an open chromatin state and gene expression in embryos and placenta.

806 In this study we modeled how genetic-epigenetic interactions in the paternal germline can
807 synergize in response to obesity to worsen metabolic dysfunction in descendants. The enhanced
808 phenotypes observed in the descendants of obese F₀ TG revealed an increased susceptibility to the
809 HFD in the TG line. An explanation for this response is that the F₀ TG were descendants from a
810 lineage with pre-existing alterations in the sperm epigenome due to the genetic modification
811 causing KDM1A overexpression. This genetic stress in combination with the environmental
812 challenge of the HFD resulted in a uniquely altered sperm epigenome in comparison to the WT,
813 and worsened offspring phenotypes. Notably, paternal obesity-induced transgenerational
814 metabolic disturbances in offspring were only observed in descendants of obese TG males. This
815 transgenerational effect may be attributed to TG KDM1A obese sires having a pre-existing altered
816 sperm epigenome at regions that escape reprogramming (Lismer *et al.*, 2020). In support of this

817 rationale that a subset of H3K4me3 regions in sperm are conserved across generations, is the
818 observed continuity in liver gene expression alterations from the F₀-F₂.

819 In the context of this study, our findings suggest that transgenerational inheritance via the
820 paternal germline is exceptional. Indeed, the phenomena of transgenerational inheritance has been
821 most documented in genetic mouse models of epigenetic inheritance and studied in relation to
822 DNA methylation patterns. These include the Avy agouti model (Morgan *et al.*, 1999; Dolinoy *et*
823 *al.*, 2006; Cropley *et al.*, 2016), the kinky tail model (Axin^{Fu} allele) (Rakyan *et al.*, 2003), and in
824 mice bearing a mutation in the *Mtrr* gene, a folate metabolism enzyme (Padmanabhan *et al.*, 2013).
825 In the context of environmental challenges, paternal transgenerational inheritance has been
826 associated with altered sperm DNA methylation when there has been gestational exposure to
827 toxicants and undernutrition (Anway *et al.*, 2005; Martínez *et al.*, 2014), and in a non-genetic
828 pharmacologically-induced prediabetes model begun at weaning (Wei *et al.*, 2014). Taken
829 together, this growing body of evidence indicates that transgenerational inheritance occurs under
830 genetic influence, or when exposures coincide with developmental programming. The male F₀
831 mice in this study were exposed to the paternal HFD from weaning and not *in utero*, which may
832 account for why transgenerational effects were not observed in WT HFD descendants. Another
833 possibility is that transgenerational responses in the WT may have become detectable in older
834 mice.

835 Our analysis indicates that the inherited metabolic disturbances observed in adult
836 descendants originated early in development. In rodent models, paternal obesity and *in utero*
837 undernutrition has been linked to altered gene expression in offspring livers and pancreatic islets
838 with some minor links to concordant DNA methylation changes (Carone *et al.*, 2011; Martínez *et*
839 *al.*, 2014; Wei *et al.*, 2014). It has been suggested that diet-associated alterations in DNA

840 methylation in sperm are retained through embryogenesis and maintained in adult tissues
841 mediating paternally-induced phenotypes (Martínez *et al.*, 2014; Wei *et al.*, 2014). Consistent with
842 these studies, altered hepatic gene expression occurred in F₁₋₂ offspring of obese sires. In contrast,
843 we observed minimal overlap of genes and functional pathways between altered H3K4me3
844 enrichment in sperm, with those differentially expressed in F₁ livers. Instead, we demonstrate a
845 significant overlap of obese sperm H3K4me3 profiles with the expression of metabolic-related
846 genes in the embryo and placenta. Based on these findings, we suggest that the metabolic
847 phenotypes we observe originate in early embryogenesis and through changes in placental gene
848 expression.

849 There is a bounty of research linking maternal obesity to adverse metabolic consequences
850 for the offspring that coincide with altered placental gene expression and function (Kerr *et al.*,
851 2018; Franzago *et al.*, 2019). On the other hand, it is an emerging concept that the paternal
852 environment including factors such as diet and age can influence placental development and
853 function. It is known that paternally expressed genes contribute to placental growth, trophoblast
854 invasion and insulin resistance and adiposity (Moore, 2001; Binder, Hannan and Gardner, 2012;
855 Wang *et al.*, 2013; Rosenfeld, 2015; Naruse *et al.*, 2019; Michelle M Denomme *et al.*, 2020;
856 Michelle M. Denomme *et al.*, 2020). In humans, errors in epigenomic programming have been
857 associated with gestational trophoblast disease and pre-eclampsia, but the role of the obese father
858 in these conditions has been entirely unexplored (Gabory, Attig and Junien, 2011; Nelissen *et al.*,
859 2011). Previous studies support a connection between paternal diets, obesity, and placental
860 dysfunction as a developmental route to metabolic disease in children. For example, we have
861 shown that a folate deficient paternal diet and altered sperm DNA methylation coincided with
862 deregulated placenta gene expression of *Cav1* and *Txndc16* (Lambrot *et al.*, 2013). Moreover,

863 paternal obesity in mice has been attributed to defective placental development (Binder, Hannan
864 and Gardner, 2012; Binder *et al.*, 2015). In women, altered DNA methylation in the regulation of
865 some genes in preeclampsia has been established. However, many genes with deregulated
866 expression were not associated with DNA methylation raising the possibility of altered chromatin
867 signatures leading to abnormal gene expression in this placental disorder (Leavey *et al.*, 2018).
868 Indeed, upregulated expression of LncRNA by increased H3K4me3 has been observed in
869 preeclampsia placentas (Sun *et al.*, 2020), and the levels of H3K4me3 as detected by
870 immunocytochemistry are decreased (Meister *et al.*, 2021). Until now the connection between
871 sperm chromatin and placenta function has been unexplored. Our analyses revealed that most of
872 the obesity-altered H3K4me3 at promoters occurred at loci involved in placental development and
873 inflammatory processes (56.6% and 76.8% of deH3K4me3 occurred at promoters expressed in the
874 trophoctoderm and placenta, respectively). Remarkably, deregulated expression of genes
875 implicated in inflammation have been implicated in hypertensive disorders in pregnancy including
876 pre-eclampsia. This raises the possibility that the paternal sperm epigenome may influence
877 maternal health during pregnancy in addition to that of the developing fetus. Hypertensive
878 disorders in pregnancy have been associated with increased risk for developing cardiovascular
879 disease (Naruse *et al.*, 2019).

880 As in previous studies we found that paternal obesity resulted in sex-specific differences
881 in metabolism and fat accretion with males being more impacted. The underlying mechanisms
882 that lead to the greater susceptibility of males may be related to sexually dimorphic placental gene
883 expression (Eriksson *et al.*, 2010). In support of this possibility, paternal environment (diet)
884 influenced placental function in a sex-specific manner (Binder *et al.*, 2015). Alternatively,
885 different metabolic responses in male and female offspring may be due to hormonal responses

886 where estrogen has been shown to protect against altered glucose homeostasis (Gupte, Pownall
887 and Hamilton, 2015; Lainez *et al.*, 2018).

888 In summary, we provide evidence that paternal obesity induced altered H3K4me3
889 signatures in sperm that may in part contribute to the transgenerational inheritance of metabolic
890 disease. The finding that genetic-epigenetic interactions may function in disease susceptibility via
891 sperm H3K4me3 brings to light that paternal metabolic disease transmission may be heightened
892 in situations where several environmental stressors converge on the sperm epigenome. Our
893 findings indicate further studies on the relationship between sperm chromatin, the placental
894 chromatin and gene expression are warranted and could lead to a better understanding of paternal
895 sperm epigenome transmission of metabolic disease. The translational validation of these findings
896 will be important in developing intervention strategies focused on paternal health that could impact
897 the health of future generations (Barratt *et al.*, 2021).

898

899 REFERENCES

900 Alexa, A., Rahnenführer, J. and Lengauer, T. (2006) 'Improved scoring of functional groups
901 from gene expression data by decorrelating GO graph structure', *Bioinformatics*, 22(13), pp.
902 1600–1607. doi: 10.1093/bioinformatics/btl140.

903 Anway, M. D. *et al.* (2005) 'Epigenetic Transgenerational Actions of Endocrine Disruptors and
904 Male Fertility', *Science*, 308(5727), pp. 1466 LP – 1469. doi: 10.1126/science.1108190.

905 Ayala, J. E. *et al.* (2010) 'Standard operating procedures for describing and performing
906 metabolic tests of glucose homeostasis in mice', *DMM Disease Models and Mechanisms*, 3(9–
907 10), pp. 525–534. doi: 10.1242/dmm.006239.

908 Barratt, C. L. R. *et al.* (2021) 'A global approach to addressing the policy, research and social

909 challenges of male reproductive health.’, *Human reproduction open*, 2021(1), p. hoab009. doi:
910 10.1093/hropen/hoab009.

911 Benjamini, Y. and Hochberg, Y. (1995) ‘Controlling the False Discovery Rate: A Practical and
912 Powerful Approach to Multiple Testing’, *Journal of the Royal Statistical Society. Series B*
913 *(Methodological)*. [Royal Statistical Society, Wiley], 57(1), pp. 289–300. Available at:
914 <http://www.jstor.org/stable/2346101>.

915 Binder, N. K. *et al.* (2015) ‘Paternal obesity in a rodent model affects placental gene expression
916 in a sex-specific manner’, *Reproduction*, 149(5), pp. 435–444. doi: 10.1530/REP-14-0676.

917 Binder, N. K., Hannan, N. J. and Gardner, D. K. (2012) ‘Paternal Diet-Induced Obesity Retards
918 Early Mouse Embryo Development, Mitochondrial Activity and Pregnancy Health’, *PLoS ONE*,
919 7(12). doi: 10.1371/journal.pone.0052304.

920 Bolger, A. M., Lohse, M. and Usadel, B. (2014) ‘Trimmomatic : a flexible trimmer for Illumina
921 sequence data’, *Bioinformatics*, 30(15), pp. 2114–2120. doi: 10.1093/bioinformatics/btu170.

922 Braun, J. M., Messerlian, C. and Hauser, R. (2017) ‘Fathers Matter: Why It’s Time to Consider
923 the Impact of Paternal Environmental Exposures on Children’s Health.’, *Current epidemiology*
924 *reports*, 4(1), pp. 46–55. doi: 10.1007/s40471-017-0098-8.

925 Brionne, A., Juanchich, A. and Hennequet-Antier, C. (2019) ‘ViSEAGO: A Bioconductor
926 package for clustering biological functions using Gene Ontology and semantic similarity’,
927 *BioData Mining*. *BioData Mining*, 12(1), pp. 1–13. doi: 10.1186/s13040-019-0204-1.

928 Brown, C. L. *et al.* (2015) ‘Addressing Childhood Obesity: Opportunities for Prevention.’,
929 *Pediatric clinics of North America*, 62(5), pp. 1241–1261. doi: 10.1016/j.pcl.2015.05.013.

930 Brykczynska, U. *et al.* (2010) ‘Repressive and active histone methylation mark distinct
931 promoters in human and mouse spermatozoa’, *Nature Structural and Molecular Biology*. *Nature*

- 932 Publishing Group, 17(6), pp. 679–687. doi: 10.1038/nsmb.1821.
- 933 Carone, B. R. *et al.* (2010) ‘Paternally induced transgenerational environmental reprogramming
934 of metabolic gene expression in mammals’, *Cell*. Elsevier Inc., 143(7), pp. 1084–1096. doi:
935 10.1016/j.cell.2010.12.008.
- 936 Carone, B. R. *et al.* (2011) ‘Paternally-induced transgenerational environmental reprogramming
937 of metabolic gene expression in mammals Benjamin’, 143(7), pp. 1084–1096. doi:
938 10.1016/j.cell.2010.12.008.Paternally-induced.
- 939 de Castro Barbosa, T. *et al.* (2016) ‘High-fat diet reprograms the epigenome of rat spermatozoa
940 and transgenerationally affects metabolism of the offspring’, *Molecular Metabolism*. Elsevier
941 GmbH, 5(3), pp. 184–197. doi: 10.1016/j.molmet.2015.12.002.
- 942 Cavalcante, R. G. and Sartor, M. A. (2017) ‘annotatr: genomic regions in context.’,
943 *Bioinformatics (Oxford, England)*, 33(15), pp. 2381–2383. doi: 10.1093/bioinformatics/btx183.
- 944 Chen, Q. *et al.* (2016) ‘Sperm tsRNAs contribute to intergenerational inheritance of an acquired
945 metabolic disorder’, *Science*, 351(6271), pp. 397–400. doi: 10.1126/science.aad7977.
- 946 Chu, A. *et al.* (2019) ‘The Placental Transcriptome in Late Gestational Hypoxia Resulting in
947 Murine Intrauterine Growth Restriction Parallels Increased Risk of Adult Cardiometabolic
948 Disease.’, *Scientific reports*, 9(1), p. 1243. doi: 10.1038/s41598-018-37627-y.
- 949 Conway, J. R., Lex, A. and Gehlenborg, N. (2017) ‘UpSetR: an R package for the visualization
950 of intersecting sets and their properties’, *Bioinformatics*, 33(18), pp. 2938–2940. doi:
951 10.1093/bioinformatics/btx364.
- 952 Cropley, J. E. *et al.* (2016) ‘Male-lineage transmission of an acquired metabolic phenotype
953 induced by grand-paternal obesity’, *Molecular Metabolism*. Elsevier GmbH, 5(8), pp. 699–708.
954 doi: 10.1016/j.molmet.2016.06.008.

- 955 Dalgaard, K. *et al.* (2016) ‘Trim28 Haploinsufficiency Triggers Bi-stable Epigenetic Obesity’,
956 *Cell*. Elsevier, 164(3), pp. 353–364. doi: 10.1016/j.cell.2015.12.025.
- 957 Denomme, Michelle M. *et al.* (2020) ‘Advanced paternal age directly impacts mouse embryonic
958 placental imprinting’, *PLoS ONE*, 15(3), pp. 1–13. doi: 10.1371/journal.pone.0229904.
- 959 Denomme, Michelle M *et al.* (2020) ‘The inherited methylome landscape is directly altered with
960 paternal aging and associated with offspring neurodevelopmental disorders’, *Aging Cell*. John
961 Wiley & Sons, Ltd, 19(8), p. e13178. doi: <https://doi.org/10.1111/accel.13178>.
- 962 Dolinoy, D. C. *et al.* (2006) ‘Maternal genistein alters coat color and protects Avy mouse
963 offspring from obesity by modifying the fetal epigenome’, *Environmental Health Perspectives*,
964 114(4), pp. 567–572. doi: 10.1289/ehp.8700.
- 965 Donkin, I. *et al.* (2016) ‘Obesity and bariatric surgery drive epigenetic variation of spermatozoa
966 in humans’, *Cell Metabolism*, 23(2), pp. 369–378. doi: 10.1016/j.cmet.2015.11.004.
- 967 Donkin, I. and Barrès, R. (2018) ‘Sperm epigenetics and influence of environmental factors’,
968 *Molecular Metabolism*, 14, pp. 1–11. doi: <https://doi.org/10.1016/j.molmet.2018.02.006>.
- 969 Eberle, C. *et al.* (2020) ‘Paternal metabolic and cardiovascular programming of their offspring:
970 A systematic scoping review.’, *PloS one*, 15(12), p. e0244826. doi:
971 10.1371/journal.pone.0244826.
- 972 Eriksson, J. G. *et al.* (2010) ‘Boys live dangerously in the womb.’, *American journal of human
973 biology : the official journal of the Human Biology Council*, 22(3), pp. 330–335. doi:
974 10.1002/ajhb.20995.
- 975 Franzago, M. *et al.* (2019) ‘Nutrigenetics , epigenetics and gestational diabetes : consequences in
976 mother and child’, *Epigenetics*. Taylor & Francis, 14(3), pp. 215–235. doi:
977 10.1080/15592294.2019.1582277.

- 978 Fullston, T. *et al.* (2013) ‘Paternal obesity initiates metabolic disturbances in two generations of
979 mice with incomplete penetrance to the F2 generation and alters the transcriptional profile of
980 testis and sperm microRNA content’, *FASEB Journal*, 27(10), pp. 4226–4243. doi:
981 10.1096/fj.12-224048.
- 982 Gabory, A., Attig, L. and Junien, C. (2011) ‘Developmental programming and epigenetics’, *The
983 American Journal of Clinical Nutrition*, 94(suppl_6), pp. 1943S-1952S. doi:
984 10.3945/ajcn.110.000927.
- 985 Gel, B. *et al.* (2016) ‘regioneR: an R/Bioconductor package for the association analysis of
986 genomic regions based on permutation tests’, *Bioinformatics*, 32(2), pp. 289–291. doi:
987 10.1093/bioinformatics/btv562.
- 988 Gerdes, P. *et al.* (2016) ‘Transposable elements in the mammalian embryo: pioneers surviving
989 through stealth and service.’, *Genome biology*, 17, p. 100. doi: 10.1186/s13059-016-0965-5.
- 990 Gernand, A. D. *et al.* (2016) ‘Micronutrient deficiencies in pregnancy worldwide: health effects
991 and prevention.’, *Nature reviews. Endocrinology*, 12(5), pp. 274–289. doi:
992 10.1038/nrendo.2016.37.
- 993 Grandjean, V. *et al.* (2015) ‘RNA-mediated paternal heredity of diet-induced obesity and
994 metabolic disorders’, *Scientific Reports*. Nature Publishing Group, 5(June), pp. 1–9. doi:
995 10.1038/srep18193.
- 996 Gupte, A. A., Pownall, H. J. and Hamilton, D. J. (2015) ‘Estrogen : An Emerging Regulator of
997 Insulin Action and Mitochondrial Function’, 2015.
- 998 Hammoud, S. S. *et al.* (2009) ‘Distinctive chromatin in human sperm packages genes for embryo
999 development’, *Nature*. Nature Publishing Group, 460(7254), pp. 473–478. doi:
1000 10.1038/nature08162.

- 1001 Harris, C. R. *et al.* (2020) ‘Array programming with NumPy’, *Nature*, 585(7825), pp. 357–362.
1002 doi: 10.1038/s41586-020-2649-2.
- 1003 Hisano, M. *et al.* (2013) ‘Genome-wide chromatin analysis in mature mouse and human
1004 spermatozoa’, *Nature Protocols*, 8(12), pp. 2449–2470. doi: 10.1038/nprot.2013.145.
- 1005 Hunter, J. D. (2007) ‘Matplotlib: A 2D Graphics Environment’, *Computing in Science &
1006 Engineering*, 9(3), pp. 90–95. doi: 10.1109/MCSE.2007.55.
- 1007 Huypens, P. *et al.* (2016) ‘Epigenetic germline inheritance of diet-induced obesity and insulin
1008 resistance’, *Nature Genetics*, 48(5), pp. 497–499. doi: 10.1038/ng.3527.
- 1009 Ignatiadis, N. *et al.* (2016) ‘Data-driven hypothesis weighting increases detection power in
1010 genome-scale multiple testing’, *Nature Methods*, 13(7), pp. 577–580. doi: 10.1038/nmeth.3885.
- 1011 Isganaitis, E., Suehiro, H. and Cardona, C. (2017) ‘Who’s your daddy?: paternal inheritance of
1012 metabolic disease risk.’, *Current opinion in endocrinology, diabetes, and obesity*. England,
1013 24(1), pp. 47–55. doi: 10.1097/MED.0000000000000307.
- 1014 Jukam, D., Shariati, S. A. M. and Skotheim, J. M. (2017) ‘Zygotic Genome Activation in
1015 Vertebrates.’, *Developmental cell*, 42(4), pp. 316–332. doi: 10.1016/j.devcel.2017.07.026.
- 1016 Jung, Y. H. *et al.* (2017) ‘Chromatin States in Mouse Sperm Correlate with Embryonic and
1017 Adult Regulatory Landscapes’, *Cell Reports*. ElsevierCompany., 18(6), pp. 1366–1382. doi:
1018 10.1016/j.celrep.2017.01.034.
- 1019 Kaati, G., Bygren, L. O. and Edvinsson, S. (2002) ‘Cardiovascular and diabetes mortality
1020 determined by nutrition during parents’ and grandparents’ slow growth period’, *European
1021 Journal of Human Genetics*, 10(11), pp. 682–688. doi: 10.1038/sj.ejhg.5200859.
- 1022 Karatela, R. A. and Sainani, G. S. (2009) ‘Plasma homocysteine in obese, overweight and
1023 normal weight hypertensives and normotensives.’, *Indian heart journal*. India, 61(2), pp. 156–

1024 159.

1025 Kerr, B. *et al.* (2018) ‘Foetoplacental epigenetic changes associated with maternal metabolic
1026 dysfunction.’, *Placenta*. Netherlands, 69, pp. 146–152. doi: 10.1016/j.placenta.2018.04.006.

1027 Kim, D., Langmead, B. and Salzberg, S. L. (2015) ‘HISAT: a fast spliced aligner with low
1028 memory requirements’, *Nature Methods*, 12(4), pp. 357–360. doi: 10.1038/nmeth.3317.

1029 Kolde, R. (2019) ‘pheatmap: Pretty Heatmaps. R package’. Available at: [https://cran.r-](https://cran.r-project.org/package=pheatmap)
1030 [project.org/package=pheatmap](https://cran.r-project.org/package=pheatmap).

1031 Krueger, F. (2015) ‘Trim galore’, *A wrapper tool around Cutadapt and FastQC to consistently*
1032 *apply quality and adapter trimming to FastQ files*, 516, p. 517.

1033 Krueger, F. and Andrews, S. R. (2016) ‘SNPsplit: Allele-specific splitting of alignments between
1034 genomes with known SNP genotypes [version 1; referees: 3 approved]’, *F1000Research*, 5, pp.
1035 1–15. doi: 10.12688/F1000RESEARCH.9037.1.

1036 Lainez, N. M. *et al.* (2018) ‘Diet-induced obesity elicits macrophage infiltration and reduction in
1037 spine density in the hypothalami of male but not female mice’, *Frontiers in Immunology*,
1038 9(SEP), pp. 1–16. doi: 10.3389/fimmu.2018.01992.

1039 Lambrot, R. *et al.* (2013) ‘Low paternal dietary folate alters the mouse sperm epigenome and is
1040 associated with negative pregnancy outcomes’, *Nature Communications*, 4. doi:
1041 10.1038/ncomms3889.

1042 Lambrot, R. *et al.* (2019) ‘The genomic distribution of histone H3K4me2 in spermatogonia is
1043 highly conserved in sperm†.’, *Biology of reproduction*. United States, 100(6), pp. 1661–1672.
1044 doi: 10.1093/biolre/ioz055.

1045 Lambrot, R. (2021) ‘Whole genome sequencing of H3 lysine 4 tri-methylation and DNA
1046 methylation in human sperm reveals regions of overlap and exclusion linked to fertility,

1047 development and epigenetic inheritance’, *Cell Reports*, CELL-REPOR.

1048 Leavey, K. *et al.* (2018) ‘Epigenetic regulation of placental gene expression in transcriptional
1049 subtypes of preeclampsia’, *Clinical Epigenetics*, 10(1), p. 28. doi: 10.1186/s13148-018-0463-6.

1050 Leek, J. T. *et al.* (2012) ‘The sva package for removing batch effects and other unwanted
1051 variation in high-throughput experiments.’, *Bioinformatics (Oxford, England)*, 28(6), pp. 882–
1052 883. doi: 10.1093/bioinformatics/bts034.

1053 Lesch, B. J. *et al.* (2019) ‘Intergenerational epigenetic inheritance of cancer susceptibility in
1054 mammals’, *eLife*, 8, pp. 1–29. doi: 10.7554/elife.39380.

1055 Li, H. *et al.* (2009) ‘The Sequence Alignment/Map format and SAMtools.’, *Bioinformatics*
1056 *(Oxford, England)*, 25(16), pp. 2078–2079. doi: 10.1093/bioinformatics/btp352.

1057 Lismer, A. *et al.* (2020) ‘Sperm histone H3 lysine 4 trimethylation is altered in a genetic mouse
1058 model of transgenerational epigenetic inheritance’, *Nucleic Acids Research*. doi:
1059 10.1093/nar/gkaa712.

1060 Lismer, A., Lambrot, R., *et al.* (2021) ‘ChIP-seq protocol for sperm cells and embryos to assess
1061 environmental impacts and epigenetic inheritance’, *STAR Protocols*, 2(2), p. 100602. doi:
1062 <https://doi.org/10.1016/j.xpro.2021.100602>.

1063 Lismer, A., Dumeaux, V., *et al.* (2021) ‘Histone H3 lysine 4 trimethylation in sperm is
1064 transmitted to the embryo and associated with diet- induced phenotypes in the offspring Article
1065 Histone H3 lysine 4 trimethylation in sperm is transmitted to the embryo and associated with
1066 diet-induce’, *Developmental Cell*. Elsevier Inc., pp. 1–16. doi: 10.1016/j.devcel.2021.01.014.

1067 Liu, L. *et al.* (2019) ‘An integrated chromatin accessibility and transcriptome landscape of
1068 human pre-implantation embryos’, *Nature communications*. Nature Publishing Group UK, 10(1),
1069 p. 364. doi: 10.1038/s41467-018-08244-0.

- 1070 Liu, X. *et al.* (2016) ‘Distinct features of H3K4me3 and H3K27me3 chromatin domains in pre-
1071 implantation embryos’, *Nature*. Nature Publishing Group, 537(7621), pp. 558–562. doi:
1072 10.1038/nature19362.
- 1073 Love, M. I., Huber, W. and Anders, S. (2014) ‘Moderated estimation of fold change and
1074 dispersion for RNA-seq data with DESeq2’, *Genome Biology*, 15(12), pp. 1–21. doi:
1075 10.1186/s13059-014-0550-8.
- 1076 Lumey, L. H. and Poppel, F. W. A. Van (2013) ‘The Dutch Famine of 1944-45 as a Human
1077 Laboratory : Changes in the Early Life Environment and Adult Health’, in Lumey, L. H. and
1078 Vaiserman, A. (ed.) *Early Life Nutrition and Adult Health and Development*. Nova Science
1079 Publishers, Inc., pp. 59–76.
- 1080 Lun, A. T. L. and Smyth, G. K. (2016) ‘csaw: a Bioconductor package for differential binding
1081 analysis of ChIP-seq data using sliding windows.’, *Nucleic acids research*, 44(5), p. e45. doi:
1082 10.1093/nar/gkv1191.
- 1083 Martínez, D. *et al.* (2014) ‘In utero undernutrition in male mice programs liver lipid metabolism
1084 in the second-generation offspring involving altered Lxra DNA methylation.’, *Cell metabolism*.
1085 United States, 19(6), pp. 941–951. doi: 10.1016/j.cmet.2014.03.026.
- 1086 Mckinney, W. (2010) ‘Data Structures for Statistical Computing in Python’, in *Proceedings of*
1087 *the 9th Python in Science Conference*, pp. 56–61.
- 1088 Meister, S. *et al.* (2021) ‘Epigenetic modification via H3K4me3 and H3K9ac in human placenta
1089 is reduced in preeclampsia’, *Journal of Reproductive Immunology*, 145, p. 103287. doi:
1090 <https://doi.org/10.1016/j.jri.2021.103287>.
- 1091 Miska, E. A. and Ferguson-smith, A. C. (2016) ‘Transgenerational inheritance: Models and
1092 mechanisms of non – DNA sequence – based inheritance’, 354(6308), pp. 778–782.

- 1093 Moore, T. (2001) ‘Genetic conflict, genomic imprinting and establishment of the epigenotype in
1094 relation to growth.’, *Reproduction (Cambridge, England)*. England, 122(2), pp. 185–193. doi:
1095 10.1530/rep.0.1220185.
- 1096 Morgan, H. D. *et al.* (1999) ‘Epigenetic inheritance at the agouti locus in the mouse’, *Nature*
1097 *Genetics*, 23(3), pp. 314–318. doi: 10.1038/15490.
- 1098 *Mouse Genome Informatics* (no date).
- 1099 Naruse, K. *et al.* (2019) ‘Preliminary evidence of a paternal-maternal genetic conflict on the
1100 placenta: Link between imprinting disorder and multi-generational hypertensive disorders’,
1101 *Placenta*, 84, pp. 69–73. doi: <https://doi.org/10.1016/j.placenta.2019.02.009>.
- 1102 Nelissen, E. C. M. *et al.* (2011) ‘Epigenetics and the placenta’, *Human Reproduction Update*,
1103 17(3), pp. 397–417. doi: 10.1093/humupd/dmq052.
- 1104 Ng, S.-F. *et al.* (2010) ‘Chronic high-fat diet in fathers programs β -cell dysfunction in female rat
1105 offspring’, *Nature*, 467(7318), pp. 963–966. doi: 10.1038/nature09491.
- 1106 Oksanen, J. *et al.* (2007) ‘The vegan package’, *Community ecology package*, 10(631–637), p.
1107 719.
- 1108 Padmanabhan, N. *et al.* (2013) ‘Mutation in Folate Metabolism Causes Epigenetic Instability and
1109 Transgenerational Effects on Development’, *Cell*. Elsevier Inc., 155(1), pp. 81–93. doi:
1110 10.1016/j.cell.2013.09.002.
- 1111 Palmer, N. O. *et al.* (2011) ‘SIRT6 in mouse spermatogenesis is modulated by diet-induced
1112 obesity.’, *Reproduction, fertility, and development*. Australia, 23(7), pp. 929–939. doi:
1113 10.1071/RD10326.
- 1114 Pembrey, M. E. *et al.* (2006) ‘Sex-specific, male-line transgenerational responses in humans’,
1115 *European Journal of Human Genetics*, 14(2), pp. 159–166. doi: 10.1038/sj.ejhg.5201538.

- 1116 Perez-Garcia, V. *et al.* (2018) ‘Placentation defects are highly prevalent in embryonic lethal
1117 mouse mutants’, *Nature*, 555(7697), pp. 463–468. doi: 10.1038/nature26002.
- 1118 Pertea, M. *et al.* (2015) ‘StringTie enables improved reconstruction of a transcriptome from
1119 RNA-seq reads’, *Nature Biotechnology*, 33(3), pp. 290–295. doi: 10.1038/nbt.3122.
- 1120 Pilsner, J. R. *et al.* (2021) ‘Aging-induced changes in sperm DNA methylation are modified by
1121 low dose of perinatal flame retardants’, *Epigenomics. Future Medicine*, 13(4), pp. 285–297. doi:
1122 10.2217/epi-2020-0404.
- 1123 Pohl, A. and Beato, M. (2014) ‘bwtool: a tool for bigWig files’, *Bioinformatics*, 30(11), pp.
1124 1618–1619. doi: 10.1093/bioinformatics/btu056.
- 1125 Radford, E. J. *et al.* (2014) ‘In utero undernourishment perturbs the adult sperm methylome and
1126 intergenerational metabolism’, *Science*, 345(6198), p. 1255903. doi: 10.1126/science.1255903.
- 1127 Rakyan, V. K. *et al.* (2003) ‘Transgenerational inheritance of epigenetic states at the murine
1128 AxinFu allele occurs after maternal and paternal transmission’, *Proceedings of the National
1129 Academy of Sciences of the United States of America*, 100(5), pp. 2538–2543. doi:
1130 10.1073/pnas.0436776100.
- 1131 Ramírez, F. *et al.* (2016) ‘deepTools2: a next generation web server for deep-sequencing data
1132 analysis.’, *Nucleic acids research*, 44(W1), pp. W160-5. doi: 10.1093/nar/gkw257.
- 1133 Ritchie, M. E. *et al.* (2015) ‘limma powers differential expression analyses for RNA-sequencing
1134 and microarray studies.’, *Nucleic acids research*, 43(7), p. e47. doi: 10.1093/nar/gkv007.
- 1135 Rosenfeld, C. S. (2015) ‘Sex-Specific Placental Responses in Fetal Development’,
1136 *Endocrinology*, 156(10), pp. 3422–3434. doi: 10.1210/en.2015-1227.
- 1137 Salas-Huetos, A. *et al.* (2021) ‘Sperm DNA methylation changes after short-term nut
1138 supplementation in healthy men consuming a Western-style diet.’, *Andrology. England*, 9(1), pp.

1139 260–268. doi: 10.1111/andr.12911.

1140 Sales, V. M., Ferguson-Smith, A. C. and Patti, M. E. (2017) ‘Epigenetic Mechanisms of
1141 Transmission of Metabolic Disease across Generations’, *Cell Metabolism*. Elsevier Inc., 25(3),
1142 pp. 559–571. doi: 10.1016/j.cmet.2017.02.016.

1143 Salzberg, B. L. and S. L. (2013) ‘Fast gapped-read alignment with Bowtie 2’, *Nature Methods*,
1144 9(4), pp. 357–359. doi: 10.1038/nmeth.1923.Fast.

1145 Sánchez-Margalet, V. *et al.* (2002) ‘Elevated plasma total homocysteine levels in
1146 hyperinsulinemic obese subjects’, *The Journal of Nutritional Biochemistry*, 13(2), pp. 75–79.
1147 doi: [https://doi.org/10.1016/S0955-2863\(01\)00197-8](https://doi.org/10.1016/S0955-2863(01)00197-8).

1148 Sharma, U. *et al.* (2016) ‘Biogenesis and function of tRNA fragments during sperm maturation
1149 and fertilization in mammals’, 351(6271), pp. 391–396. doi:
1150 10.1126/science.aad6780.Biogenesis.

1151 Shen, L. (2014) ‘GeneOverlap : An R package to test and visualize gene overlaps’, pp. 1–10.

1152 Shen, Y. *et al.* (2012) ‘A map of the cis-regulatory sequences in the mouse genome.’, *Nature*,
1153 488(7409), pp. 116–120. doi: 10.1038/nature11243.

1154 Siklenka, K. *et al.* (2015) ‘Disruption of histone methylation in developing sperm impairs
1155 offspring health transgenerationally’, *Science*, 350(6261). doi: 10.1126/science.aab2006.

1156 Soubry, A. *et al.* (2016) ‘Obesity-related DNA methylation at imprinted genes in human sperm:
1157 Results from the TIEGER study’, *Clinical Epigenetics*, 8(1), p. 51. doi: 10.1186/s13148-016-
1158 0217-2.

1159 Stringer, J. M. *et al.* (2018) ‘Reduced PRC2 function alters male germline epigenetic
1160 programming and paternal inheritance’, *BMC Biology*. BMC Biology, 16(1), pp. 1–20. doi:
1161 10.1186/s12915-018-0569-5.

- 1162 Sun, N. *et al.* (2020) ‘H3K4me3-Mediated Upregulation of LncRNA-HEIPP in Preeclampsia
1163 Placenta Affects Invasion of Trophoblast Cells’, 11(December), pp. 1–11. doi:
1164 10.3389/fgene.2020.559478.
- 1165 Taiyun, Wei, Simko, V. (2021) ‘R package “corrplot”: Visualization of a Correlation Matrix.’
1166 Available at: <https://github.com/taiyun/corrplot>.
- 1167 Team, R. C. (2018) ‘R: A language and environment for statistical computing.’ Vienna, Austria:
1168 R Foundation for Statistical Computing.
- 1169 Voight, B. F. *et al.* (2010) ‘Twelve type 2 diabetes susceptibility loci identified through large-
1170 scale association analysis’, *Nature Genetics*, 42(7), pp. 579–589. doi: 10.1038/ng.609.
- 1171 Wang, X. *et al.* (2013) ‘Paternal expressed genes predominate in the placenta’, *Proceedings of*
1172 *the National Academy of Sciences*, 110(26), pp. 10705–10710. doi: 10.1073/pnas.1308998110.
- 1173 Waskom, M. L. (2021) ‘seaborn : statistical data visualization Statement of need’, *The Journal of*
1174 *Open Source Software*, 6, pp. 1–4. doi: 10.21105/joss.03021.
- 1175 Wei, Y. *et al.* (2014) ‘Paternal induced transgenerational inheritance of susceptibility to
1176 diabetes in mammals’, *Proceedings of the National Academy of Sciences*, 111(5), pp. 1873–
1177 1878. doi: 10.1073/pnas.1321195111.
- 1178 Welch, R. P. *et al.* (2014) ‘ChIP-Enrich: gene set enrichment testing for ChIP-seq data’, *Nucleic*
1179 *Acids Research*, 42(13), pp. e105–e105. doi: 10.1093/nar/gku463.
- 1180 Wickham, H. (2016) *ggplot2: Elegant Graphics for Data Analysis*. New York: Springer-Verlag.
1181 Available at: <https://ggplot2.tidyverse.org>.
- 1182 Wu, H. *et al.* (2017) ‘Preconception urinary phthalate concentrations and sperm DNA
1183 methylation profiles among men undergoing IVF treatment: a cross-sectional study.’, *Human*
1184 *reproduction (Oxford, England)*, 32(11), pp. 2159–2169. doi: 10.1093/humrep/dex283.

- 1185 Wu, J. *et al.* (2016) ‘The landscape of accessible chromatin in mammalian preimplantation
1186 embryos’, *Nature*. Nature Publishing Group, 534(7609), pp. 652–657. doi: 10.1038/nature18606.
- 1187 Yi, L. *et al.* (2018) ‘Gene-level differential analysis at transcript-level resolution’, *Genome*
1188 *Biology*. Genome Biology, 19(1), pp. 1–11. doi: 10.1186/s13059-018-1419-z.
- 1189 Yoshida, K. *et al.* (2020) ‘ATF7-Dependent Epigenetic Changes Are Required for the
1190 Intergenerational Effect of a Paternal Low-Protein Diet’, *Molecular Cell*. Elsevier Inc., 78(3), pp.
1191 445-458.e6. doi: 10.1016/j.molcel.2020.02.028.
- 1192 Youngson, N. *et al.* (2016) ‘Obesity-induced sperm DNA methylation changes at satellite repeats
1193 are reprogrammed in rat offspring YR - 2016/12/1’, *Asian Journal of Andrology*, (6 UL-
1194 [https://www.ajandrology.com/article.asp?issn=1008-](https://www.ajandrology.com/article.asp?issn=1008-682X;year=2016;volume=18;issue=6;spage=930;epage=936;aulast=Youngson;t=5)
1195 [682X;year=2016;volume=18;issue=6;spage=930;epage=936;aulast=Youngson;t=5](https://www.ajandrology.com/article.asp?issn=1008-682X;year=2016;volume=18;issue=6;spage=930;epage=936;aulast=Youngson;t=5)), pp. 930 OP-
1196 936 VO–18. doi: 10.4103/1008-682X.163190.
- 1197 Zhang, B. *et al.* (2016) ‘Allelic reprogramming of the histone modification H3K4me3 in early
1198 mammalian development’, *Nature*. Nature Publishing Group, 537(7621), pp. 553–557. doi:
1199 10.1038/nature19361.
- 1200 Zhang, Y., Parmigiani, G. and Johnson, W. E. (2020) ‘ComBat-seq: batch effect adjustment for
1201 RNA-seq count data’, *NAR Genomics and Bioinformatics*, 2(3). doi: 10.1093/nargab/lqaa078.
- 1202 Zhang, Yunfang *et al.* (2018) ‘Dnmt2 mediates intergenerational transmission of paternally
1203 acquired metabolic disorders through sperm small non-coding RNAs’, *Nature Cell Biology*.
1204 Springer US, 20(May). doi: 10.1038/s41556-018-0087-2.
- 1205
- 1206

1207 **ACKNOWLEDGEMENTS**

1208 We thank the team at the McGill University and Génome Québec Innovation Centre for
1209 performing the sequencing and Dr. Deborah Sloboda (McMaster Univeristy) for advice on
1210 metabolic phenotyping methods. This research was funded by the Canadian Institute of Health
1211 Research (CIHR) grants to SK (358654 and 350129).

1212

1213 **AUTHOR CONTRIBUTIONS**

1214 SK conceived, designed, funded and guided the study. ASP developed the model and conducted
1215 the animal studies with assistance from CL and RL with associated laboratory analysis. ASP
1216 conducted the bioinformatic analysis with assistance and oversight from VD. ASP and SK
1217 assembled and wrote the manuscript which was edited by VD.

1218

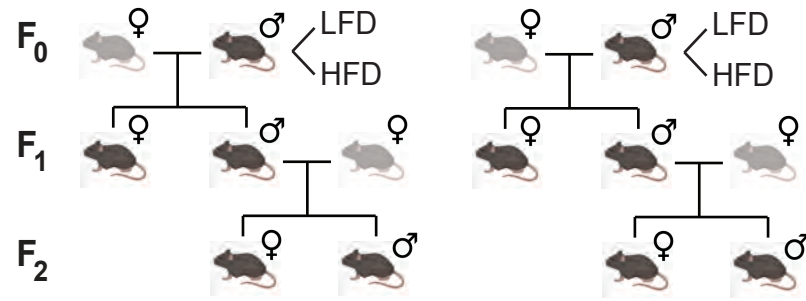
1219 **COMPETING INTEREST**

1220 The authors declare no competing interests.

A

C57BL/6NCrl WT

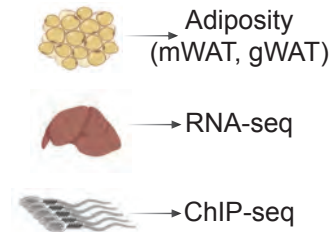
C57BL/6NCrl
KDM1A^{+/-} TG



B



C



—●— WT LFD - - - ● - - - WT HFD —●— TG LFD - - - ● - - - TG HFD

Glucose tolerance test

Insulin tolerance test

F₀♂

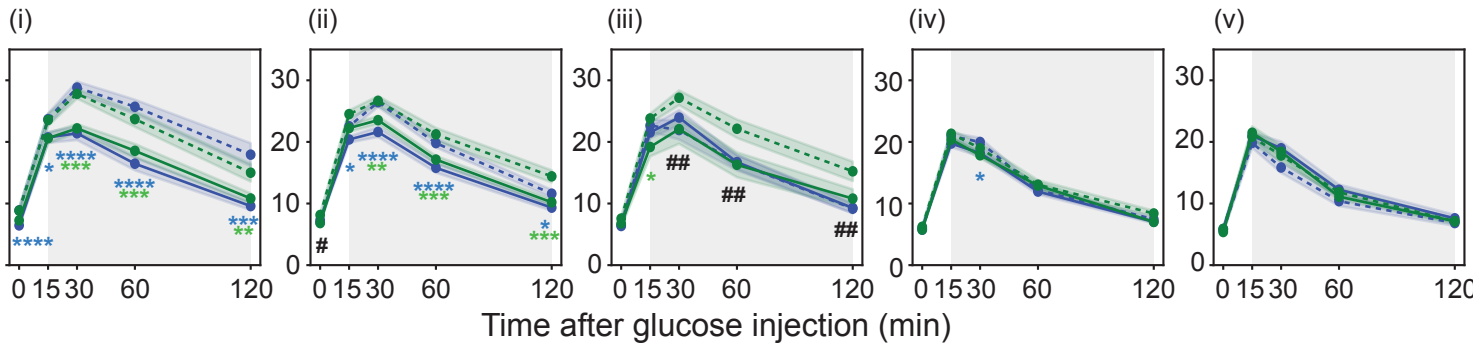
F₁♂

F₂♂

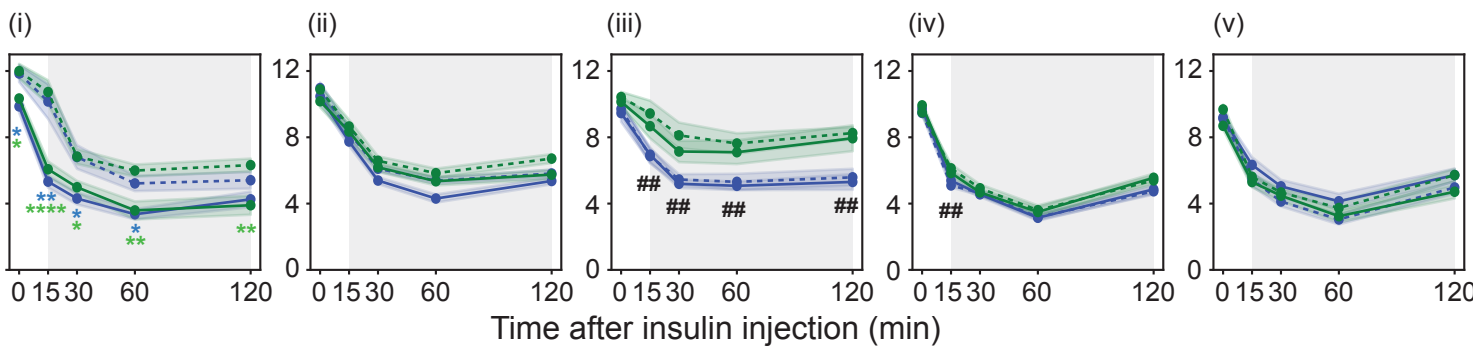
F₁♀

F₂♀

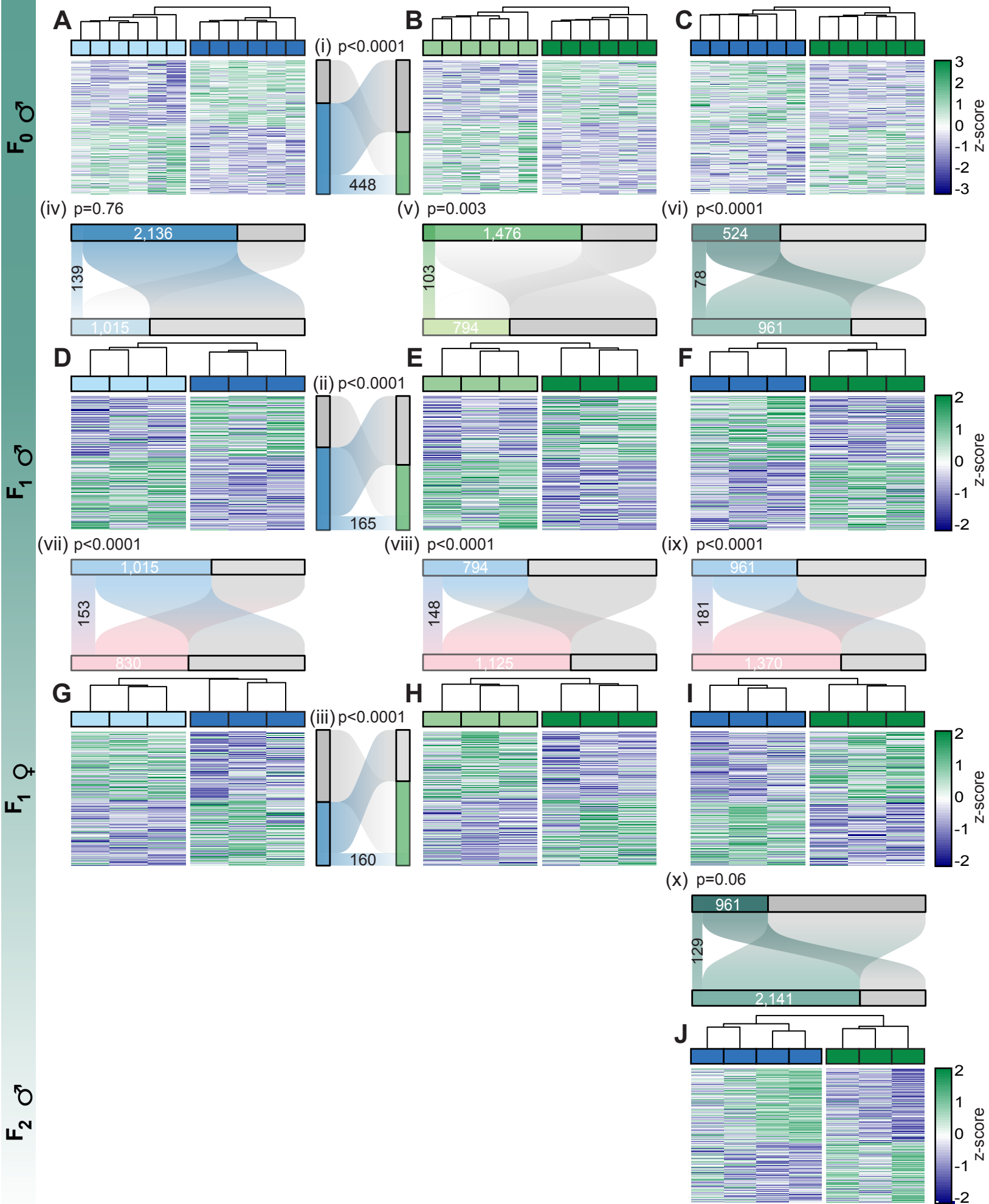
D
Blood glucose (mM)



E
Blood glucose (mM)

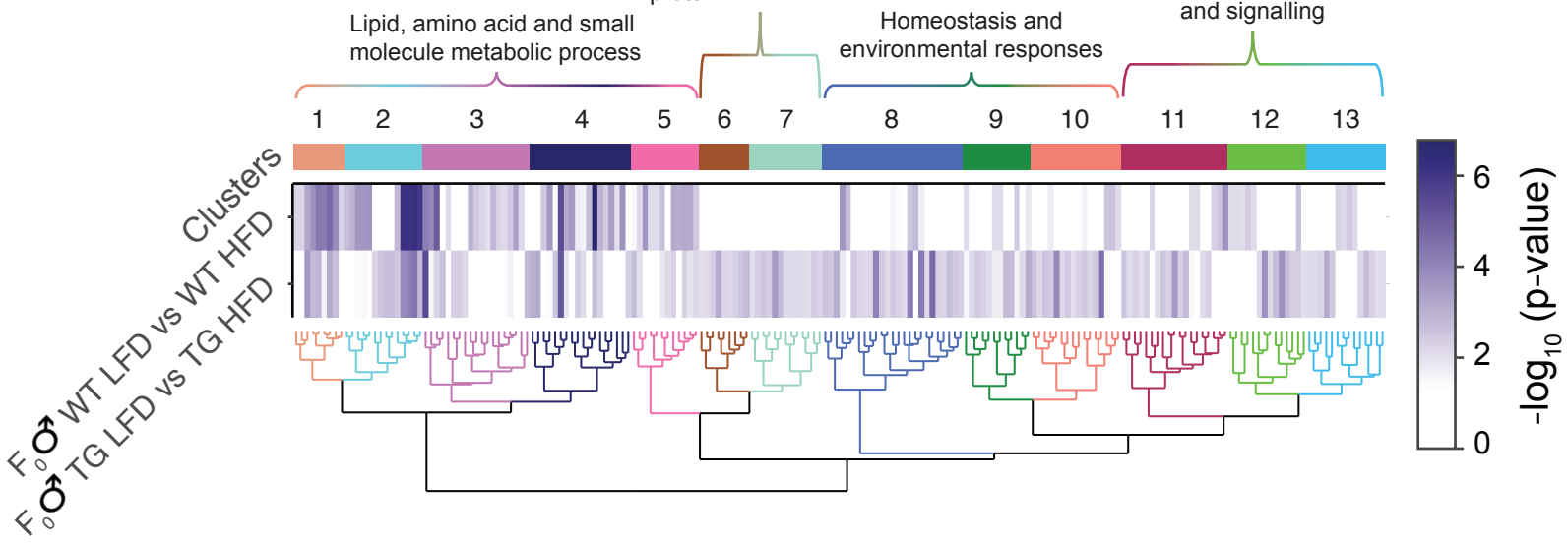


1221 **Figure 1: Paternal obesity induces transgenerational metabolic phenotypes in a sex-specific**
1222 **manner that are enhanced in KDM1A descendants** A) Experimental mouse model depicting
1223 breeding scheme and generations studied. Male C57BL6NCrI (WT) and KDM1A^{+/-} transgenics
1224 (TG, C57BL6NCrI) were fed either a low-fat diet (LFD) or high-fat diet (HFD) from weaning for
1225 10-12 weeks, then mated to 8-week-old C57BL6NCrI females fed a regular chow diet (CD).
1226 Animals studied per experimental group: F₀ (n=15-25 males), F₁ (n=28-49 per sex) and F₂ (n=8-
1227 21 per sex) B) Experimental timeline for metabolic testing and downstream experiments
1228 performed for each generation (F₀₋₂). Metabolic profiles were measured after the diet intervention
1229 at 15 weeks of age and included: baseline blood glucose, and intraperitoneal glucose and insulin
1230 tolerance tests (ipGTT and ipITT, respectively). Visceral adipose depots were weighed (mWAT:
1231 mesenteric white adipose tissue and gWAT: gonadal white adipose tissue) and the left lateral lobe
1232 of the liver used for RNA-sequencing (RNA-seq). Sperm from cauda epididymides were used for
1233 chromatin immunoprecipitation followed by sequencing (ChIP-seq), targeting histone H3 lysine 4
1234 tri-methylation (H3K4me3). C) Age-matched male mice fed either a low-fat diet (left) or a high-
1235 fat diet (right) for 12 weeks. D) Glucose tolerance test. Blood glucose levels before and after
1236 (shaded in grey) an intraperitoneal glucose injection, after overnight fasting (15 ±1 hour) at 4
1237 months of age in F₀ males (i), F₁ males (ii), F₂ males (iii), F₁ females (iv) and F₂ females (v). E)
1238 Insulin tolerance test. Blood glucose levels before and after (shaded in grey) an intraperitoneal
1239 insulin injection, after a 6-hour (±1 hour) fasting at 4 months of age in F₀ males (i), F₁ males (ii),
1240 F₂ males (iii), F₁ females (iv) and F₂ females (v). Results are shown as mean ± SEM. Statistical
1241 analyses were performed using multiple t-test with Holm-Sidak correction. *P<0.05, **P<0.01,
1242 ***P<0.001, ****P<0.0001 (in blue; WT LFD vs WT HFD, in green; TG LFD vs TG HFD) and
1243 #P<0.05, ##P<0.01 (WT HFD vs TG HFD).

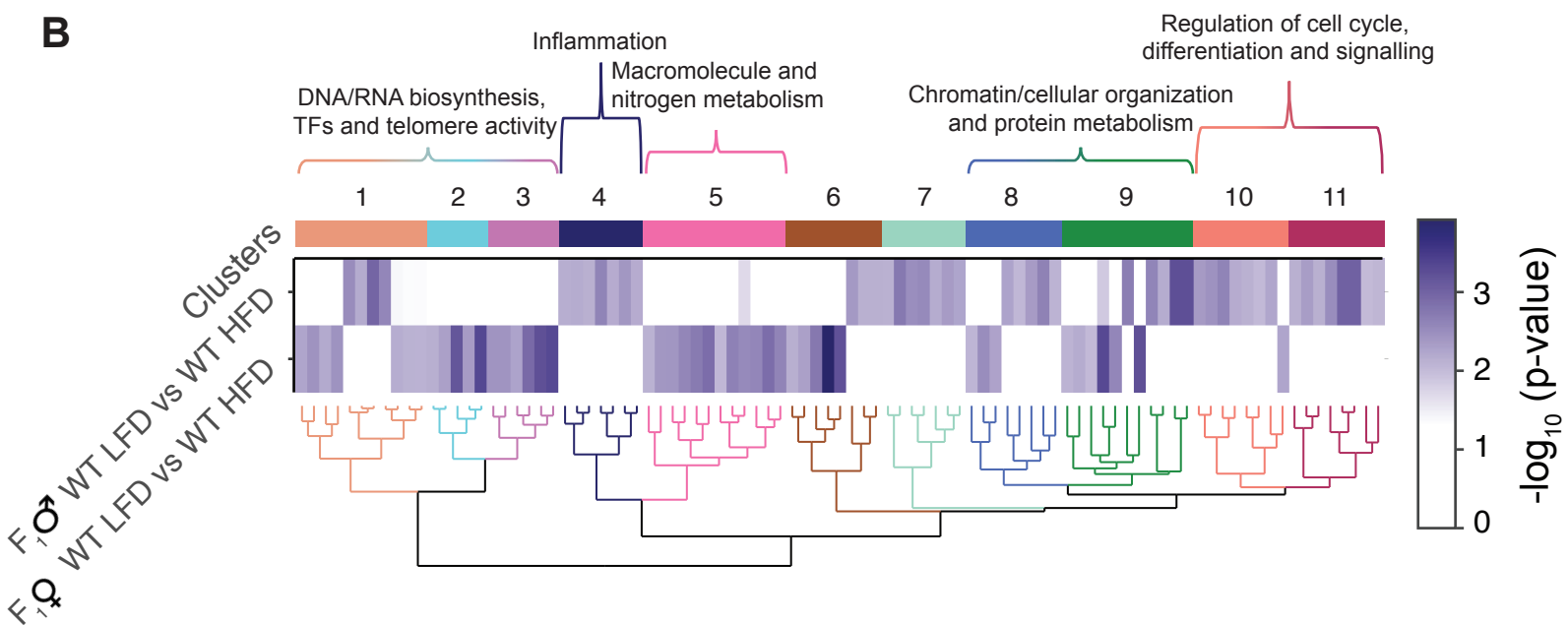


1244 **Figure 2: Paternal obesity is associated with altered gene expression in the livers of the F₀-F₂**
1245 A-J) Heatmaps of normalized expression values scaled by row (z-score) for transcripts that code
1246 for differentially expressed hepatic genes (Lancaster p-value<0.05) for each comparison assessed
1247 across sex and generation. Individual transcripts (rows) are ordered by k-means clustering and
1248 samples (columns) are arranged by hierarchical clustering, using complete-linkage clustering
1249 based on Euclidean distance. F₀ WT LFD vs WT HFD males (A), F₀ TG LFD vs TG HFD males
1250 (B), F₀ WT HFD vs TG HFD males (C), F₁ WT LFD vs WT HFD males (D), F₁ TG LFD vs TG
1251 HFD males (E), F₁ WT HFD vs TG HFD males (F), F₁ WT LFD vs WT HFD females (G), F₁ TG
1252 LFD vs TG HFD females (H), F₁ WT HFD vs TG HFD females (I), and F₂ WT HFD vs TG HFD
1253 males (J). i-x) Alluvial plots depicting frequency distributions of significant (colored boxes) and
1254 non-significant (grey boxes) genes for each comparison and their overlap across genotype (i-iii),
1255 across F₀ and F₁ males (iv-vi), across F₁ males and females (vii-ix) and across F₁ and F₂ males (x).
1256 Significance of overlap between differentially expressed genes lists was calculated by Fisher's
1257 exact test. P-values are included for each comparison above the respective alluvial plot.
1258
1259

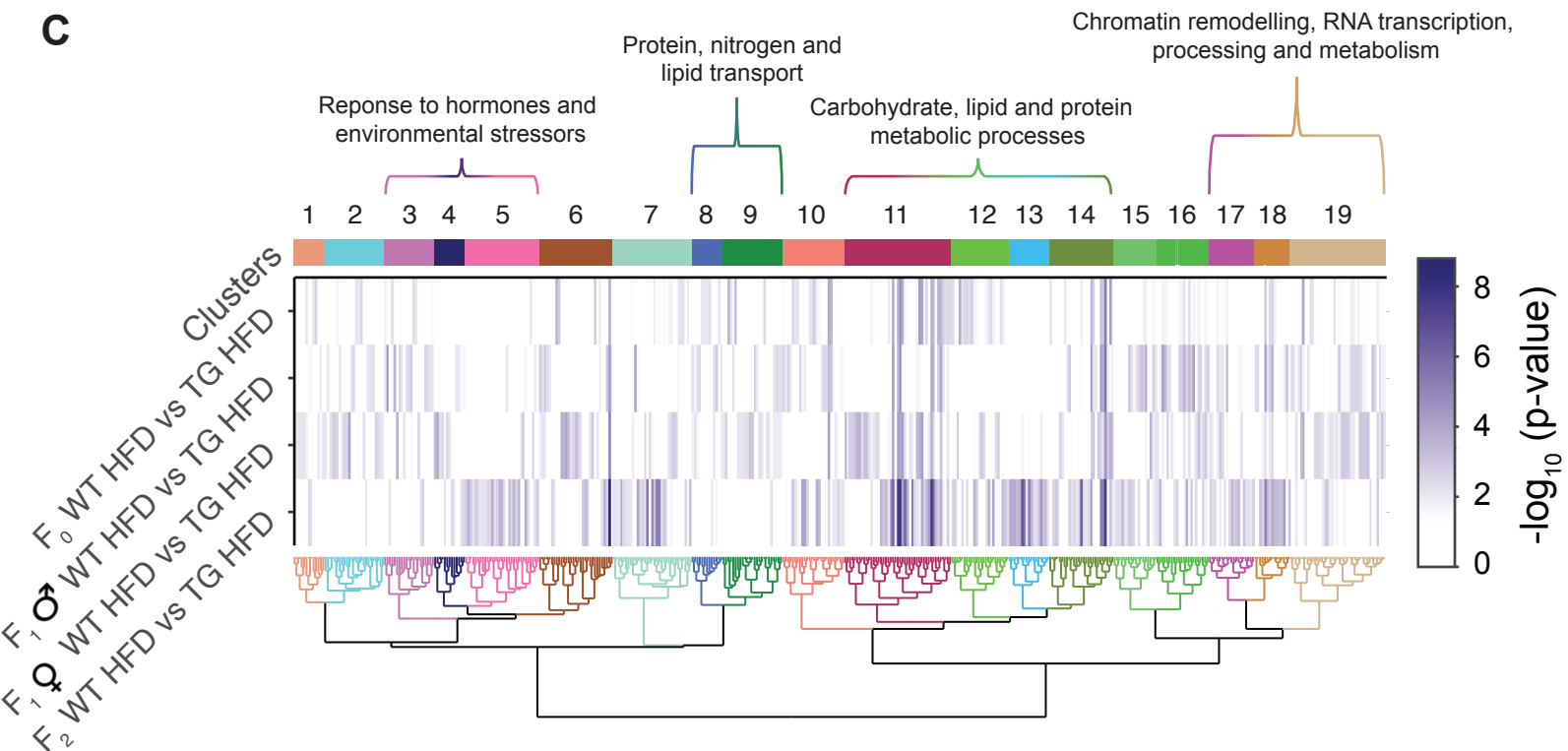
A



B

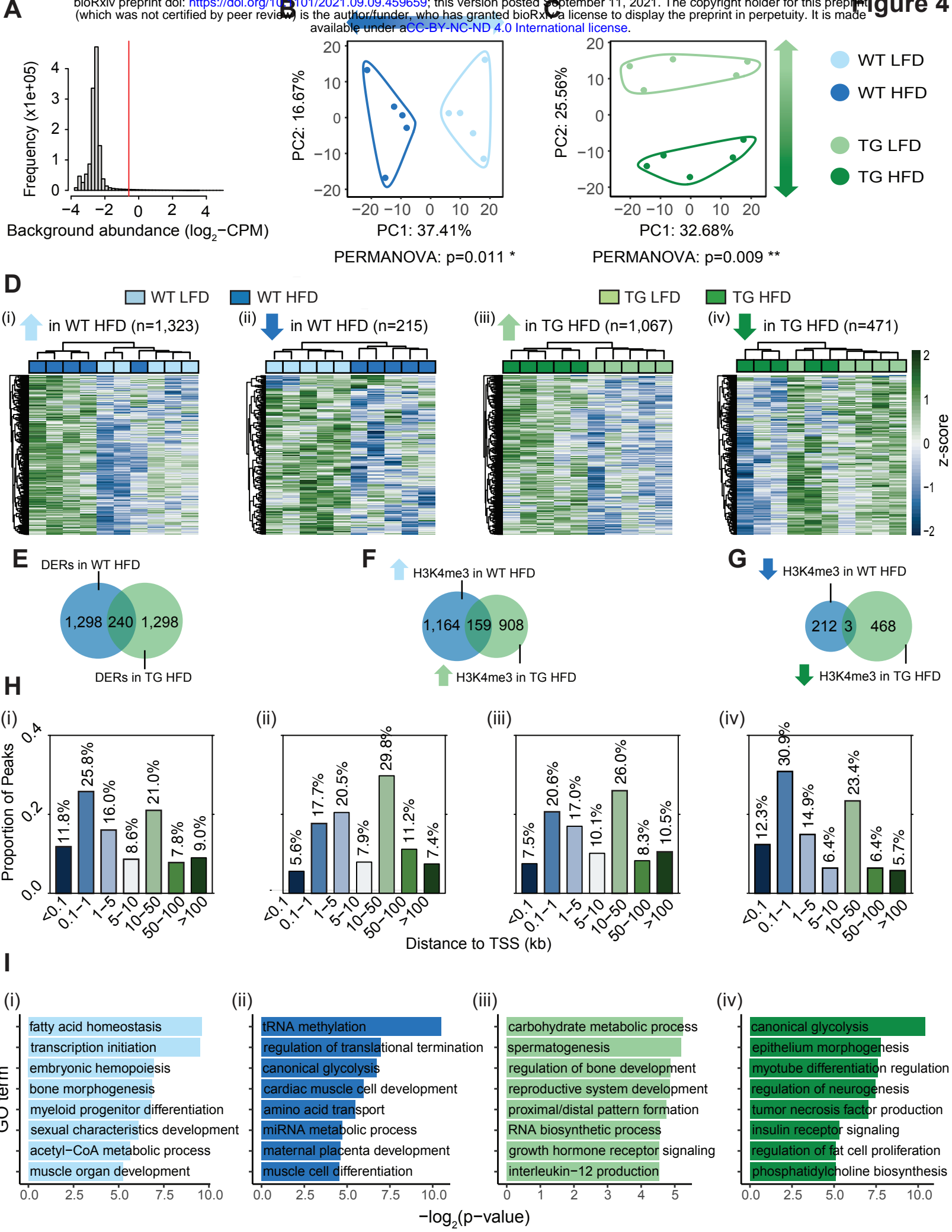


C



1260 **Figure 3: Obesity-induced hepatic transcriptome disturbances show functional similarities**
1261 **across genotype, sex and generation** A-C) Heatmaps of significant gene ontology (GO) terms
1262 clustered by functional similarity, comparing enriched biological functions for each comparison
1263 of interest across genotype (A), sex (B) and generation (C). Columns represent enriched GO terms
1264 which are ordered by hierarchical clustering based on Wang's semantic similarity distance and
1265 *ward.D2* aggregation criterion. Each row represents a comparison of interest for which enriched
1266 GO terms were annotated based on the list of significant genes. The color gradient depicts the GO
1267 term enrichment significance ($-\log_{10}$ p-value). Interactive versions of these figures can be found in
1268 Supplemental files 1-3 and the complete lists of significantly enriched GO terms can be found in
1269 Tables S3-5.
1270
1271

bioRxiv preprint doi: <https://doi.org/10.1101/2021.09.09.459659>; this version posted September 11, 2021. The copyright holder for this preprint (which was not certified by peer review) is the author/funder, who has granted bioRxiv a license to display the preprint in perpetuity. It is made available under aCC-BY-NC-ND 4.0 International license.

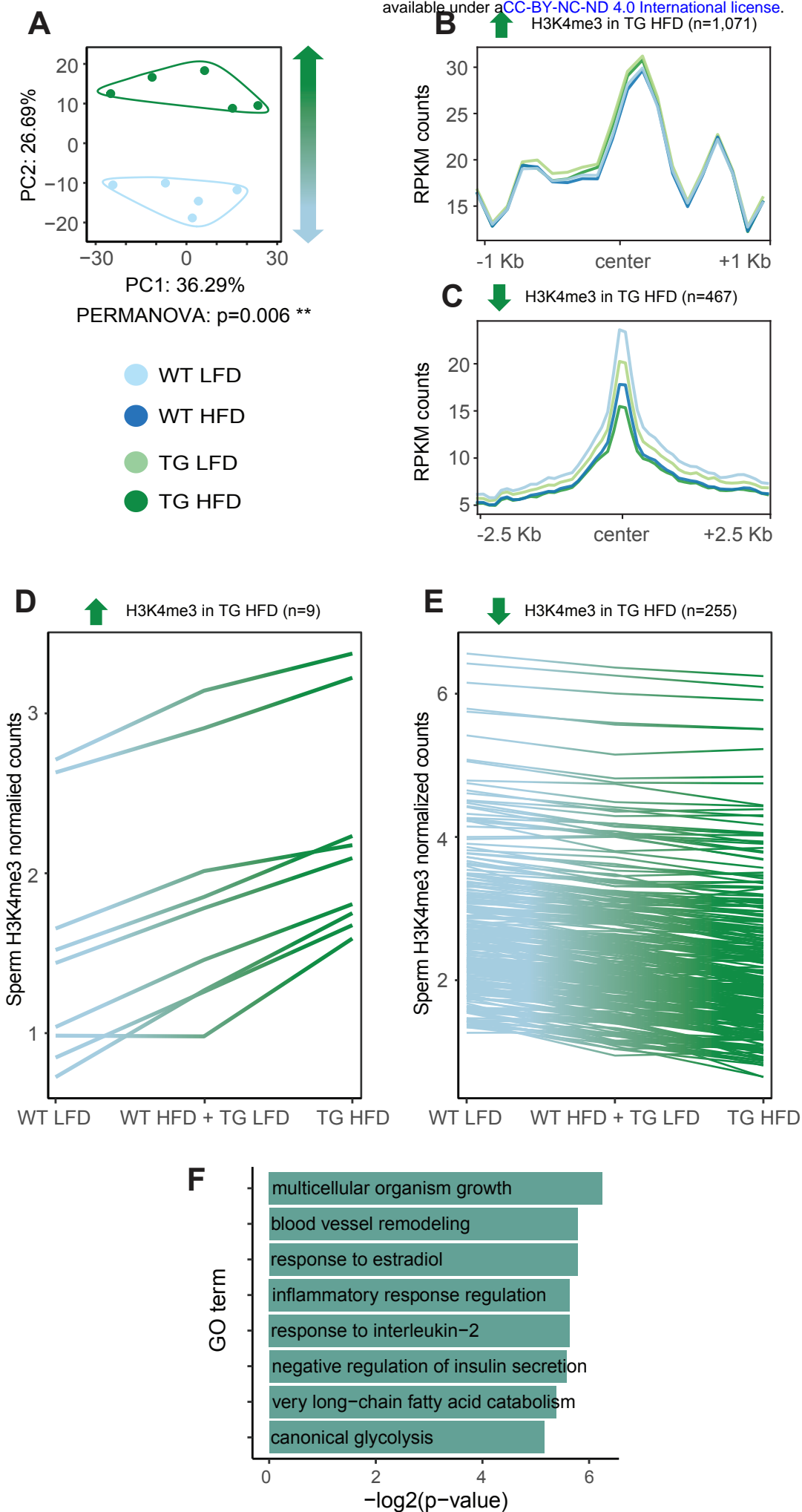


1272 **Figure 4: Genomic location, directionality change and functions of regions with altered**
1273 **H3K4me3 enrichment by obesity** A) Histogram showing frequency distributions of read
1274 abundances in 150 bp windows throughout the genome. Windows with an abundance below
1275 $\log_2(4)$ fold over background bins of 2,000 bp were filtered out as indicated by the vertical red
1276 line. Enriched regions less than 100 bp apart were merged for a maximum width of 5,000 bp,
1277 conferring a total of 30,745 merged enriched regions. Reads were counted in merged enriched
1278 regions and normalized counts were used for downstream analyses. (see Material and Methods)
1279 B-C) Principal component analysis on normalized counts at merged enriched regions comparing
1280 WT LFD vs WT HFD (B) and TG LFD vs TG HFD (C). The top 5% regions contributing to
1281 separation of samples along Principal Component 1 (in B; PC1; x axis) or PC2 (in C; y axis) were
1282 selected. The PERMANOVA p-values indicating significance associated with dietary treatment
1283 are included under each PCA plot. D) Heatmaps of \log_2 normalized counts of deH3K4me3 regions
1284 in sperm with increased enrichment in WT HFD (i; n=1,323), decreased enrichment in WT HFD
1285 (ii; n=215), increased enrichment in TG HFD (iii; n=1,067) and decreased enrichment in TG HFD
1286 (iv; n=471) in each group. Samples (columns) and regions (rows) are arranged by hierarchical
1287 clustering using complete-linkage clustering based on Euclidean distance. Colored boxes indicate
1288 sample groups (light blue=WT LFD, dark blue=WT HFD, light green=TG LFD, dark green=TG
1289 HFD). E-G). Venn diagrams showing the overlap of deH3K4me3 in sperm of WT HFD (blue) and
1290 in TG HFD (green), for all detected regions (E), those gaining H3K4me3 (F) and those losing
1291 H3K4me3 (G). H) Barplots showing the distribution of altered regions based on the distance from
1292 the TSS of the nearest gene, for regions with increased enrichment in WT HFD (i; n=1,323),
1293 decreased enrichment in WT HFD (ii; n=215), increased enrichment in TG HFD (iii; n=1,067),
1294 and decreased enrichment in TG HFD (iv; n=471). The color gradient represents the distance of

1295 the regions to TSS in kilobase. I) Gene ontology analysis of diet-induced deH3K4me3 regions at
1296 promoters with increased enrichment in WT HFD (i; n=381), decreased enrichment in WT HFD
1297 (ii; n=34), increased enrichment in TG HFD (iii; n=230) and decreased enrichment in TG HFD
1298 (iv; n=150). Barplots show 8 selected significant GO terms with their respective $-\log_2(\text{p-value})$.
1299 Tables S7-10 include the complete lists of significantly enriched GO terms.

1300

1301

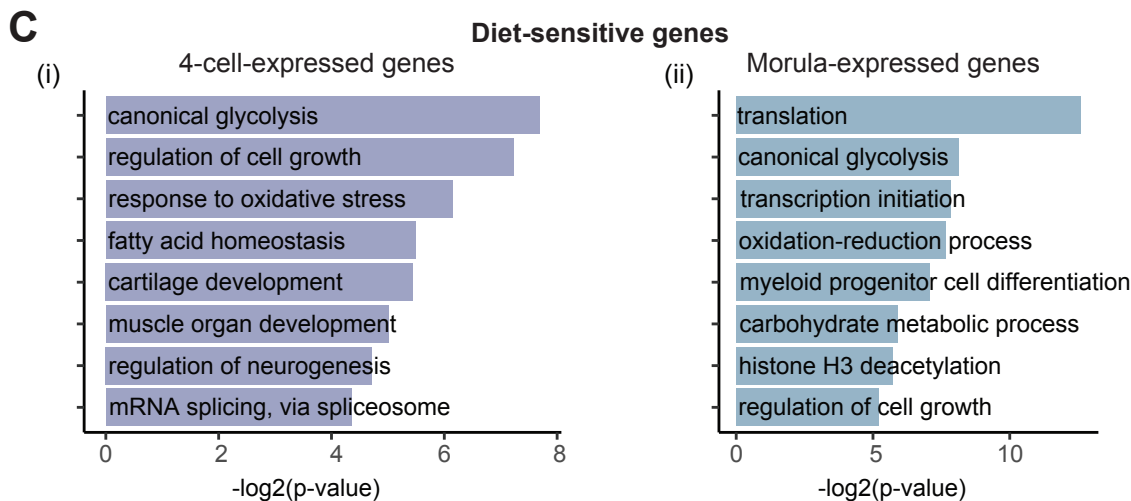
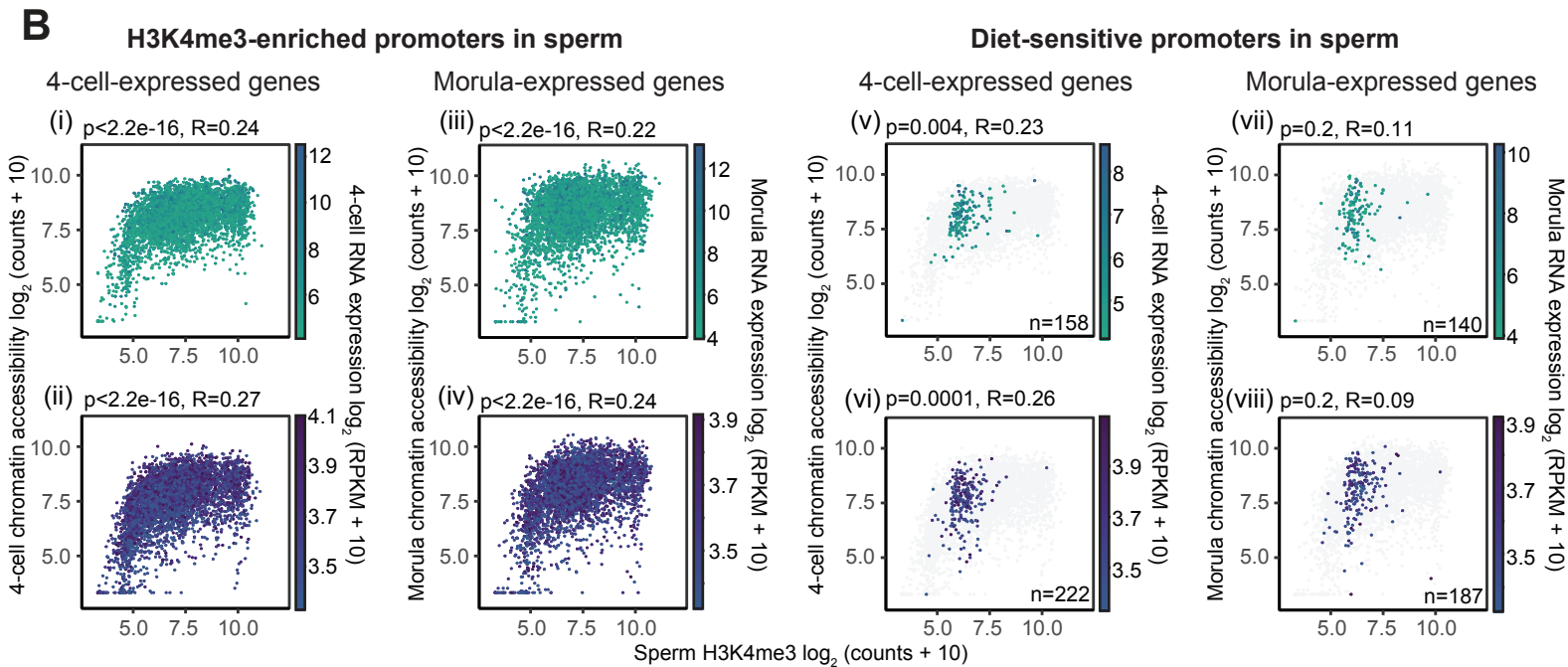
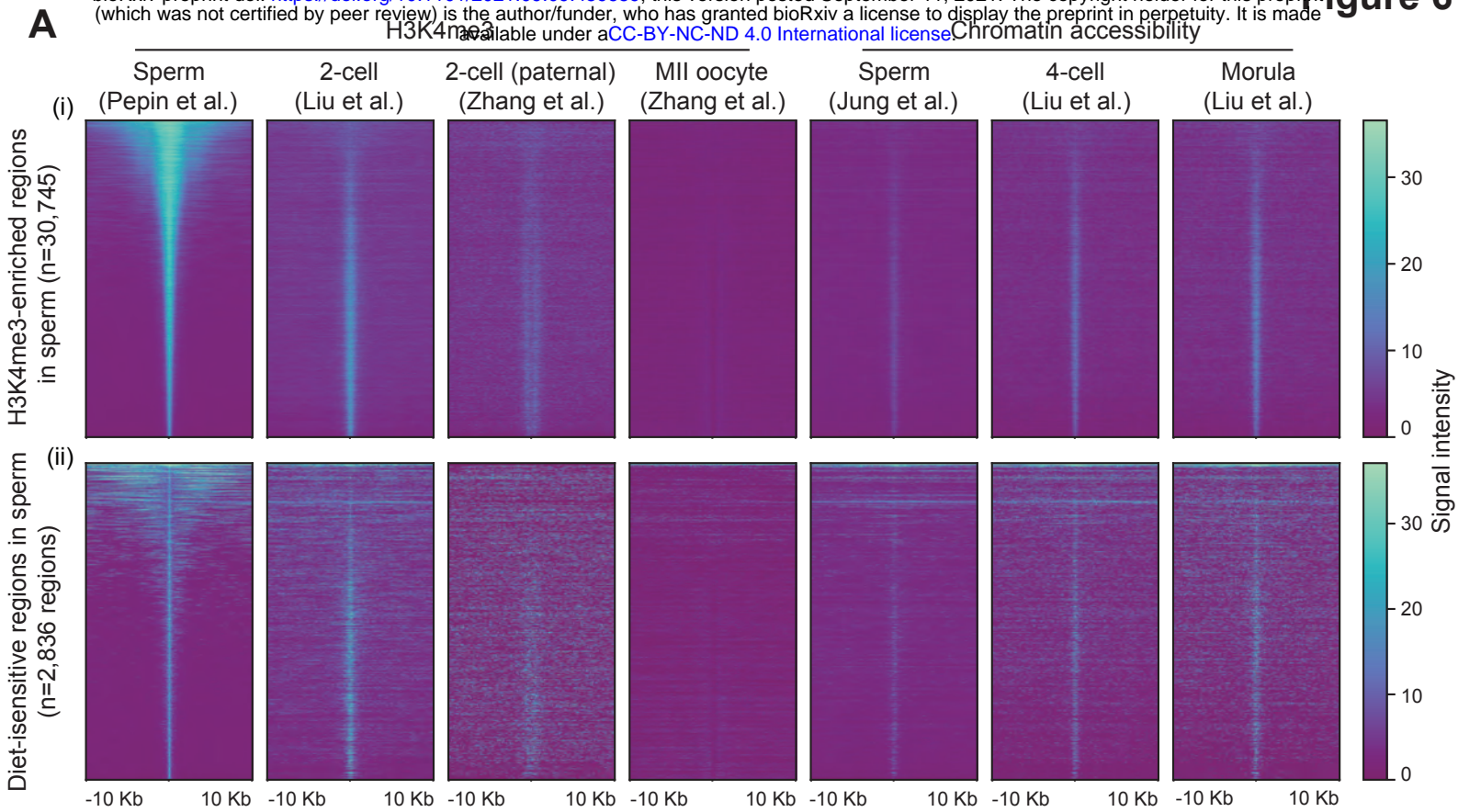


1302 **Figure 5: Additive effects of KDM1A overexpression and diet-induced obesity in the sperm**
1303 **epigenome at the level of H3K4me3**

1304 A) Principal component analysis on normalized counts at merged enriched regions comparing WT
1305 LFD vs TG HFD. The top 5% regions contributing to separation of samples along Principal
1306 Component 2 (PC2; y axis) were selected. The PERMANOVA p-value under the plot indicates
1307 significance. B-C) Profile plots of RPKM H3K4me3 counts +/- 1 kilobase around the center of
1308 regions with increased H3K4me3 (B) and +/- 2.5 kilobase around the center of regions with
1309 decreased H3K4me3 enrichment in TG HFD (C). D-E) Line plots showing the median of
1310 normalized sperm H3K4me3 counts for each experimental group at regions showing a significant
1311 trend (n=264, adjusted p-value<0.2) with a linear increase in H3K4me3 enrichment (D; n=9) or a
1312 linear decrease in H3K4me3 enrichment (E; n=255) from WT LFD, WT HFD, TG LFD to TG
1313 HFD groups. F) Gene ontology analysis on the regions associated with a significant linear trend at
1314 promoters (n=104). Barplots show 8 selected significant GO terms with their respective -log₂(p-
1315 value). Table S11 includes the complete list of significantly enriched GO terms.

1316

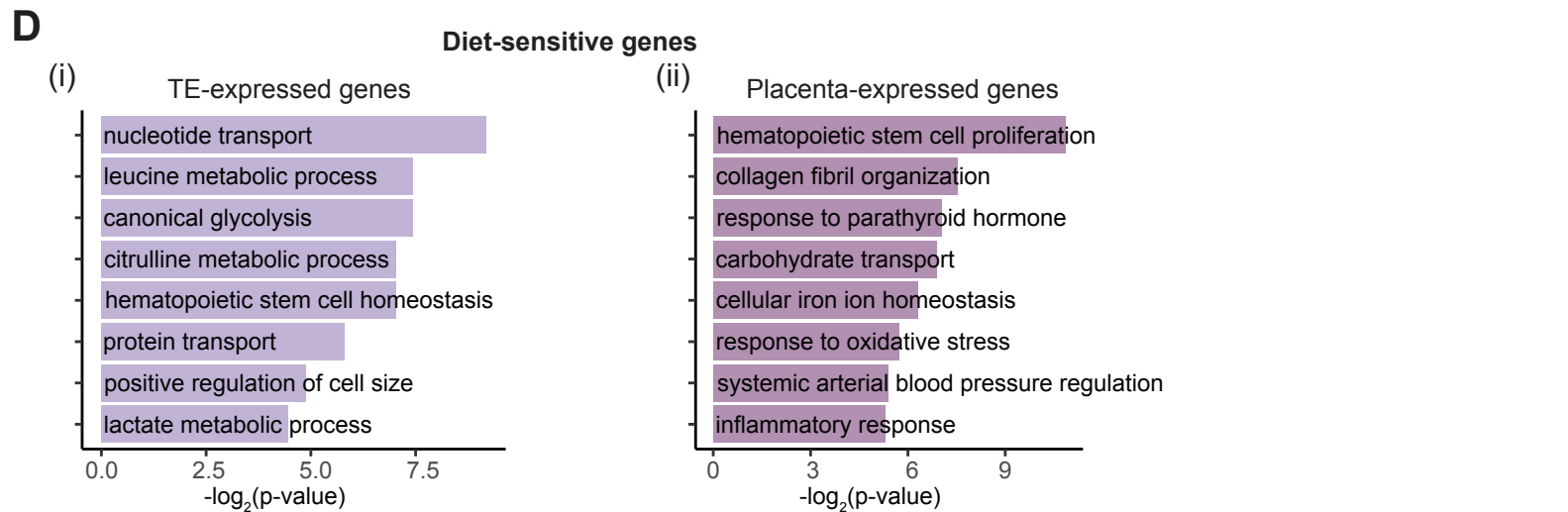
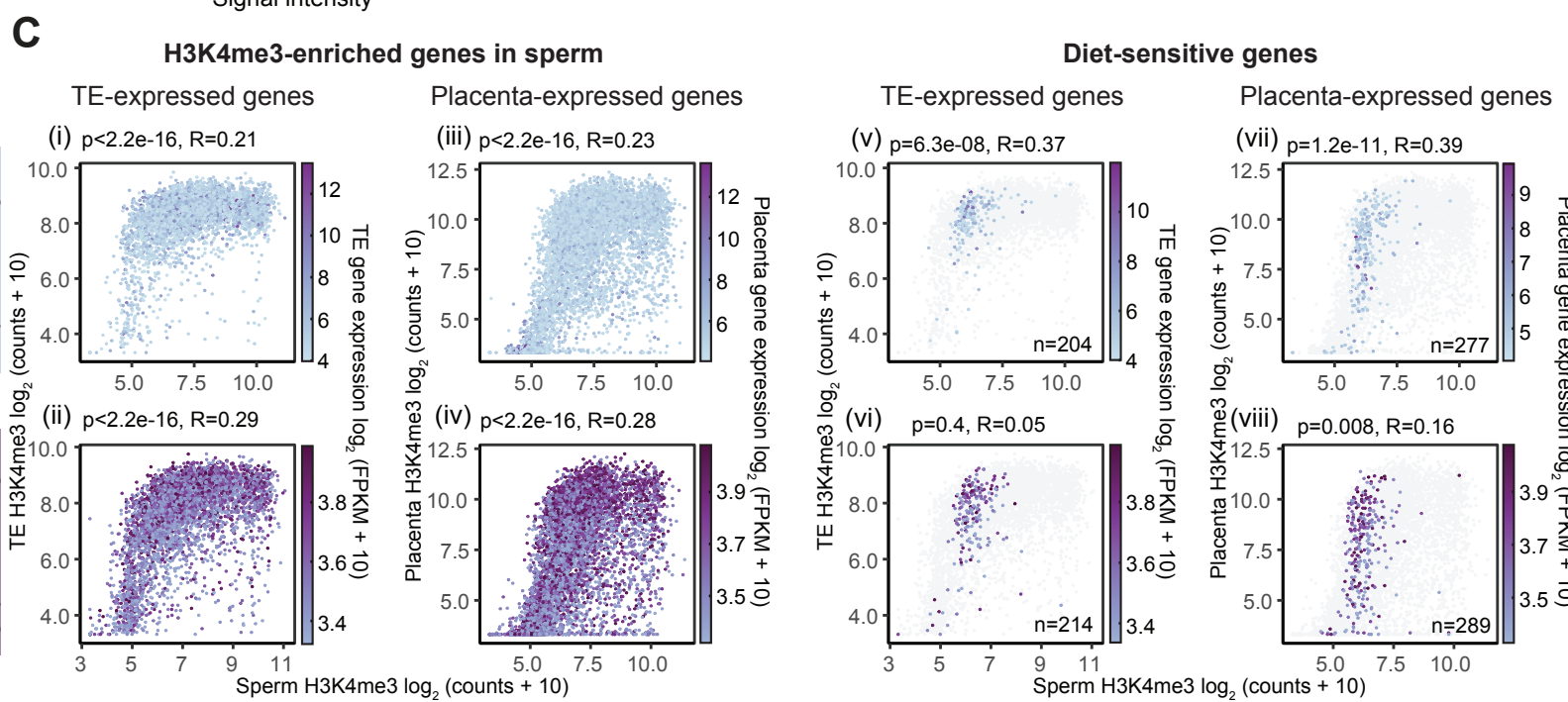
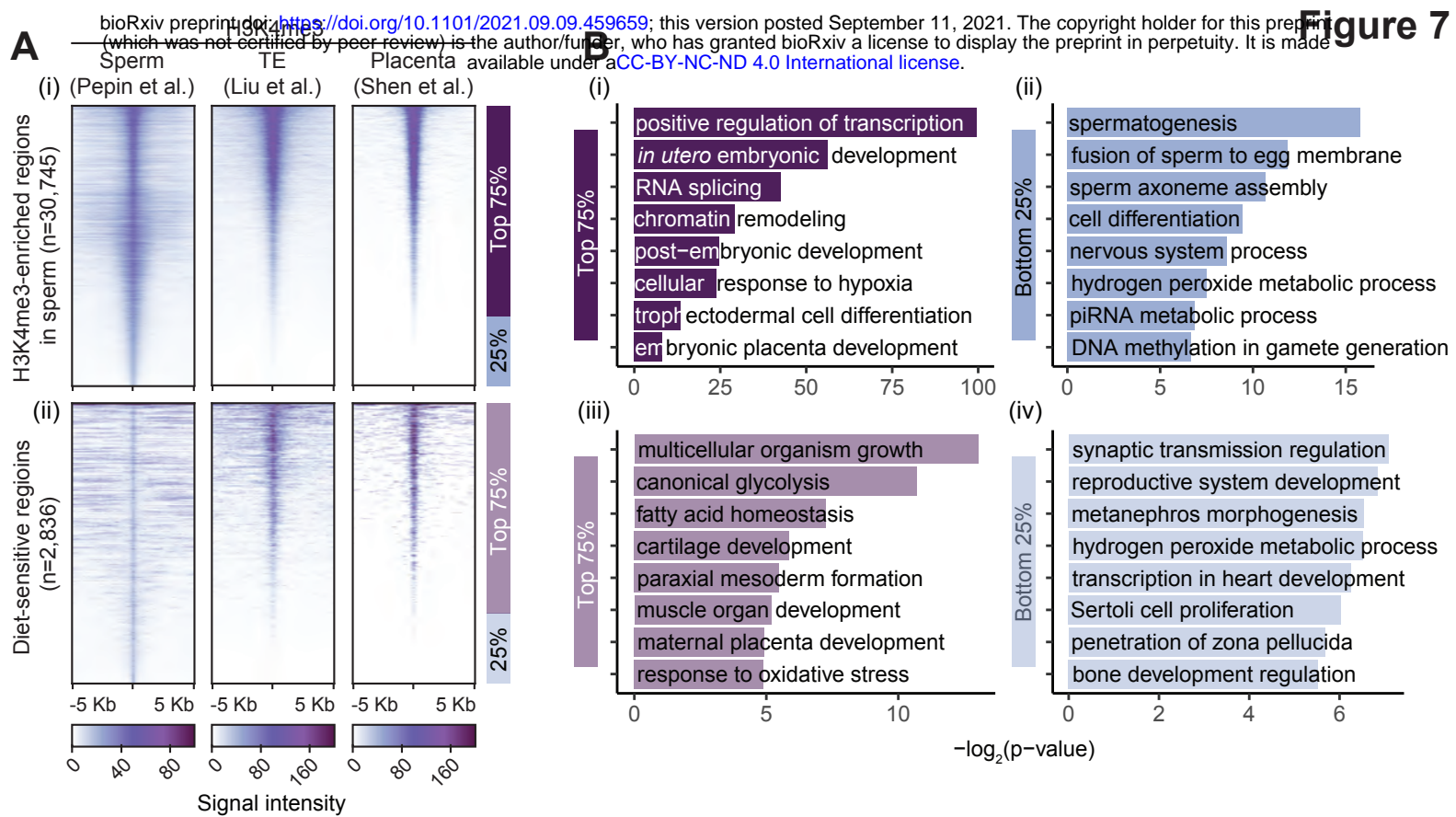
1317



1318 **Figure 6: Sperm H3K4me3 regions sensitive to obesity occur at genes with an open**
1319 **chromatin state and expressed in the pre-implantation embryo** A) Heatmaps of RPKM counts
1320 signal +/- 10 kilobase around the center of regions enriched with H3K4me3 in sperm (i; n=30,745)
1321 and regions with obesity-induced deH3K4me3 in sperm (ii; n=2,836) for H3K4me3 enrichment
1322 levels in sperm (this study), 2-cell embryo (Liu *et al.*, 2016), 2-cell embryo on the paternal allele
1323 and MII oocyte (Zhang *et al.*, 2016), and for chromatin accessibility signal in sperm (Jung *et al.*,
1324 2017), 4-cell embryo and morula embryo (Liu *et al.*, 2019). B) Scatterplots showing H3K4me3
1325 enrichment in sperm (x axis; log₂ counts + 10), chromatin accessibility signal (y axis; log₂ counts
1326 + 10; (Jung *et al.*, 2017)) and gene expression levels (color gradient; log₂ FPKM + 10; (Liu *et al.*,
1327 2019)) in 4-cell (i,ii,v,vi) or in morula (iii,iv,vii,viii) embryos, at either all genes with promoters
1328 enriched with H3K4me3 in sperm (i-iv) or at diet-sensitive genes (v-viii). The top row of
1329 scatterplots includes lowly-expressed genes (bottom 50%) in 4-cell (i and v) or morula (iii or vii)
1330 embryos. The bottom row of scatterplots includes highly-expressed genes (top 50%) in 4-cell (ii
1331 and iv) or morula (vi and viii) embryos. Pearson's correlation coefficients and their associated p-
1332 values are indicated above each scatterplot, comparing H3K4me3 enrichment in sperm versus
1333 H3K4me3 enrichment in 4-cell or morula embryos. C) Gene ontology analysis of genes expressed
1334 in the 4-cell (i) or the morula (ii) embryos, overlapping with diet-sensitive promoters in sperm.
1335 Barplots show 8 selected significant GO terms with their respective -log₂(p-value). Tables S12-13
1336 include the complete lists of significantly enriched GO terms.

1337

1338



1339 **Figure 7: Obesity-induced deH3K4me3 regions overlap with genes marked by H3K4me3 and**
1340 **expressed in the trophoctoderm and placenta** A) Heatmaps of RPKM counts signal +/- 5
1341 kilobase around the center of regions enriched with H3K4me3 in sperm (i; n=30,745) and at
1342 regions with diet-induced deH3K4me3 in sperm (n=2,836) for H3K4me3 enrichment levels in
1343 sperm (this study), trophoctoderm (TE) (Liu *et al.*, 2016) and placenta (Shen *et al.*, 2012). B) Gene
1344 ontology analysis of regions enriched with H3K4me3 in sperm, TE and placenta (top 75% from A
1345 i) (i), regions enriched with H3K4me3 in sperm only (bottom 25% from A i) (ii), diet-sensitive
1346 regions enriched with H3K4me3 in sperm, TE and placenta (top 75% from A ii) (iii), and diet-
1347 sensitive regions enriched with H3K4me3 in sperm only (bottom 25% from A ii) (iv). Barplots
1348 show 8 selected significant GO terms with their respective $-\log_2(\text{p-value})$. Tables S14-17 include
1349 the complete lists of significantly enriched GO terms. C) Scatterplots showing H3K4me3
1350 enrichment at promoters in sperm (x axis; \log_2 counts + 10), H3K4me3 enrichment (y axis; \log_2
1351 counts + 10) and gene expression levels (color gradient; \log_2 FPKM + 10) in the trophoctoderm
1352 (i,ii,v,vi; (Liu *et al.*, 2016)) or in the placenta (iii,iv,vii,viii; (Shen *et al.*, 2012; Chu *et al.*, 2019)),
1353 at either all genes with promoters enriched with H3K4me3 in sperm (i-iv) or at diet-sensitive genes
1354 (v-viii). The top row of scatterplots includes lowly-expressed genes (bottom 50%) in
1355 trophoctoderm (i and v) or placenta (iii or vii). The bottom row includes highly-expressed genes
1356 (top 50%) in trophoctoderm (ii and iv) or placenta (vi and viii). Pearson's correlation coefficients
1357 and associated p-values are indicated above each scatterplot, comparing H3K4me3 enrichment in
1358 sperm versus H3K4me3 enrichment in the trophoctoderm or placenta. D) Gene ontology analysis
1359 of genes expressed in the trophoctoderm (i) or the placenta (ii), overlapping with diet-sensitive
1360 promoters in sperm. Barplots show 8 selected significant GO terms with their respective $-\log_2(\text{p-}$
1361 $\text{value})$. Tables S18-19 include the complete lists of significantly enriched GO terms.

1364 **SUPPLEMENTAL MATERIAL TITLES**

1365 Supplemental file 1. Interactive heatmap for significant gene ontology terms enriched in livers of
1366 F0 males fed a high-fat diet across genotype, related to Figure 3A

1367

1368 Supplemental file 2. Interactive heatmap for significant gene ontology terms enriched in
1369 differentially expressed genes in livers of F1 wildtype mice descendants of obese sires across sex,
1370 related to Figure 3B

1371

1372 Supplemental file 3. Interactive heatmap for significant gene ontology terms enriched in genotype-
1373 associated differentially expressed genes in livers of animals across generation, related to Figure
1374 3C

1375

1376 Supplemental file 4. Interactive bar plot for the number of significantly enriched gene ontology
1377 terms in WT HFD vs TG HFD across generation and sex, related to Figure 3C

1378

1379 Supplemental file 5. Interactive heatmap for significant gene ontology terms enriched in at obesity-
1380 sensitive promoters in sperm and differentially expressed genes in livers of F1 males descendants
1381 of high-fat-fed sires, related to Supplemental Figure 7C

1382

1383 Table S1. Diets' macronutrients composition and energy density

1384

1385 Table S2. Number of animals used per group per sex per generation for metabolic characterization

1386

1387 Table S3. Significant gene ontology terms enriched in differentially expressed genes in livers of
1388 F0 males fed a high-fat diet across genotype, related to Figure 3A
1389
1390 Table S4. Significant gene ontology terms enriched in differentially expressed genes in livers of
1391 F1 wildtype mice descendants of obese sires across sex, related to Figure 3B
1392
1393 Table S5. Significant gene ontology terms enriched in genotype-associated differentially
1394 expressed genes in livers of animals across generation, related to Figure 3C
1395
1396 Table S6. Sperm H3K4me3 ChIP-Sequencing read numbers and alignment rates
1397
1398 Table S7. Significant gene ontology terms enriched at promoters with H3K4me3 gain in sperm of
1399 WT HFD, related to Figure 4Ii
1400
1401 Table S8. Significant gene ontology terms enriched at promoters with H3K4me3 loss in sperm of
1402 WT HFD, related to Figure 4Iii
1403
1404 Table S9. Significant gene ontology terms enriched at promoters with H3K4me3 gain in sperm of
1405 TG HFD, related to Figure 4Iiii
1406
1407 Table S10. Significant gene ontology terms enriched at promoters with H3K4me3 loss in sperm
1408 of TG HFD, related to Figure 4Iiv
1409

1410 Table S11. Significant gene ontology terms enriched at promoters associated with a significant
1411 linear trend, related to Figure 5F
1412

1413 Table S12. Significant gene ontology terms enriched at obesity-sensitive promoters of genes
1414 expressed in the 4-cell embryo, related to Figure 6Ci
1415

1416 Table S13. Significant gene ontology terms enriched at obesity-sensitive promoters of genes
1417 expressed in the morula embryo, related to Figure 6Cii
1418

1419 Table S14. Significant gene ontology terms enriched at promoters with H3K4me3 enrichment in
1420 sperm, trophoctoderm and placenta, related to Figure 7Bi
1421

1422 Table S15. Significant gene ontology terms enriched at promoters with H3K4me3 enrichment in
1423 sperm, related to Figure 7Bii
1424

1425 Table S16. Significant gene ontology terms enriched at obesity-sensitive promoters with
1426 H3K4me3 enrichment in sperm, trophoctoderm and placenta, related to Figure 7Biii
1427

1428 Table S17. Significant gene ontology terms enriched at obesity-sensitive promoters with
1429 H3K4me3 enrichment in sperm, related to Figure 7Biv
1430

1431 Table S18. Significant gene ontology terms enriched at obesity-sensitive promoters of genes
1432 expressed in the trophoctoderm, related to Figure 7Di

1433

1434 Table S19. Significant gene ontology terms enriched at obesity-sensitive promoters of genes
1435 expressed in the placenta, related to Figure 7Dii

1436

1437 Table S20. Significant gene ontology terms enriched in at obesity-sensitive promoters in sperm
1438 and differentially expressed genes in livers of F1 males descendants of high-fat-fed sires, related
1439 to Supplemental Figure 7C

1440